

# 1 Changing in the hierarchical organization of local 2 information dynamics during motor decision in the 3 premotor cortex of primates

4 Giampiero Bardella<sup>1,2</sup>, Franco Giarrocco<sup>1,2</sup>, Marta Andujar<sup>1,2</sup>, Emiliano Brunamonti<sup>2</sup>,  
5 Pierpaolo Pani<sup>2</sup>, and Stefano Ferraina<sup>2,\*</sup>

6 <sup>1</sup>PhD Program in Behavioral Neuroscience, Sapienza University of Rome, Italy

7 <sup>2</sup>Department of Physiology and Pharmacology, Sapienza University of Rome, Piazzale Aldo Moro 5, 00185, Rome,  
8 Italy

9 \*corresponding author(s): Stefano Ferraina ([stefano.ferraina@uniroma1.it](mailto:stefano.ferraina@uniroma1.it))

## 10 ABSTRACT

11 Despite recent works have investigated functional and effective cortical networks in animal models, the dynamical information transfer among functional modules underneath cognitive control is still largely unknown. Here we addressed the issue by using transfer entropy and graph theory methods on neural activities recorded from a multielectrode (96 recording sites) array in the dorsal premotor cortex of rhesus monkeys. We focused our analysis on the decision time of a stop-signal (countermanding) task. When comparing trials with successful inhibition to those with generated movement we found evidence of heterogeneous interacting modules described by 4 main classes, hierarchically organized. Interestingly, the hierarchical organization resulted different in the two type of trials. Our results suggest that motor decisions are based on the local re-organization of the premotor cortical network.

## 12 Introduction

13 The brain is a complex system formed by different interconnected modules. The definition of a module  
14 depends on the scale of analysis. At the small scale modules are single neurons, at the large scale great-  
15 specialized brain areas. In between, at the mesoscale level, modules are aggregates of neurons (populations)  
16 of different dimensions (columns; specialized sub-regions; etc). In the last fifty years, neuroscience has  
17 tried to describe brain computations by linking neural activities to behaviour. At whatever scale of neural  
18 activity investigation, crucial is the understanding of how different modules interact and how information  
19 is shared and processed among parts. In this context, the neurophysiological approach to brain functions  
20 with recording microelectrodes provided invaluable advances, mainly in animal models<sup>1</sup>. Indeed, the high  
21 spatial resolution of the method proved to be suitable for linking neurons activity to behaviour, to describe  
22 the organization of local microcircuits and, sometimes, of the over standing larger networks<sup>2,3</sup>. Most  
23 of these studies referred to the analysis of single unit (spiking) activity (SUA), others focused more on  
24 mesoscopic signals as the local field potentials (LFP) indicating the average synaptic input to the explored  
25 area (for a review see<sup>4</sup>) and, to a lesser extent, on signals sampling the average spiking activity of discrete  
26 populations<sup>5-7</sup>.

27 Here, aiming to contribute to the understanding of the role of the dorsal premotor (PMd) cortex in  
28 arm motor control<sup>8-10</sup> we studied the local spiking activity (SA) derived from a multi-electrode array and  
29 implemented a combined information-theory and topological approach to describe how the collective  
30 activity of mesoscopically-defined local modules is linked to motor decision-making. Indeed, it has been  
31 shown that neurons express more their contribution to complex behavioural functions either when observed

32 as coordinated functional ensembles<sup>11–19</sup> or described as common responses to the input they receive  
33 (e.g., the visual stimulus orientation columns<sup>20</sup>). A paradigmatic example is the interaction between  
34 fixation and movement neurons in the epochs preceding saccade generation<sup>13,14</sup>. In the present work we  
35 explored how information is managed among local modules in PMd for reaching control and how this  
36 network is arranged during either movement execution or cancellation. How different neuronal actors  
37 contribute to motor decisions is in fact still largely discussed, especially for brain centres involved in  
38 reaching control<sup>10,21</sup>. We observed that decision-making in PMd is linked to modules of information  
39 management that segregate into different classes, organize hierarchically and change in relation to the  
40 behavioural outcome. Moreover, with topological approaches, we found that the PMd network explored  
41 different configurations depending on the behavioural decision. Indeed, during movement generation,  
42 compared to movement inhibition, information transmission among modules was more efficient requiring  
43 fewer steps. This demonstrates that information among population of neurons is processed differently  
44 during the two motor behaviours explored and suggests a new perspective on the view of how the local  
45 computation evolves in motor areas during action decision-making.

## 46 Results

47 We investigated, at the mesoscopic scale, the information transfer and directed connectivity patterns among  
48 discrete populations of neurons during the motor decision phases of arm movements. To this aim we  
49 extracted a measure of the local spiking activity (SA) from each electrode of a microelectrode array (up to  
50 96 channels) in the PMd of two male Rhesus monkeys while they performed a countermanding reaching  
51 task. This task (Fig. 1) required either to move (Go trials; 67%) the arm toward a peripheral target or to  
52 cancel the movement (Stop trials; 33%) in case of appearance of a Stop signal. The two types of trials  
53 were randomly presented. During **Go trials**, after the disappearance of the central target (Go signal) the  
54 monkeys were instructed to reach the peripheral target to obtain the reward. In **Stop trials**, after the Go  
55 signal, the central target reappeared (Stop signal) after a variable delay, called SSD (Stop signal delay).  
56 In these trials the monkeys were required to refrain from moving to earn the reward (correct Stop trials).  
57 If the monkey were unable to stop, the trials were classified as wrong Stop trials, and no reward was  
58 provided. Because the SSDs were varied according to a staircase procedure based on the performance,  
59 correct Stop trials constituted approximately 50% of Stop trials (see Table 1). This task allows to estimate  
60 behaviorally the time window during which the decision to move (or to refrain) is taken. This time window  
61 is commonly referred as the stop signal reaction time (SSRT; see Table 1 for the values observed in the  
62 present study). For the analysis of the SA, among animals and recording sessions, we used a fixed epoch  
63 duration ( $T = 400$  ms). This epoch (see Figure 1; grey bar) was built on the estimated duration of the  
64 SSRT for each session plus a variable portion of time before the Stop signal appearance (see Material and  
65 Methods for details) which is irrelevant for the comparison since nothing different occur in Go trials and  
66 Stop trials during the time before the Stop signal presentation (see figure 2).

### 67 **Neural Recordings can be grouped in classes providing different contribution to the net-** 68 **work information dynamics**

69 We investigated a total of 21 recording sessions (12 for monkey P and 9 for monkey C). For each session  
70 we derived a measure of the average local spiking activity (SA; see Material and Methods), from all  
71 neurons firing in close proximity of the tip of each electrode. From now on we refer for simplicity to these  
72 discrete neuronal populations as modules.

73 Fig 2 shows, for each recording electrode of one example session, the SAs of both Go trials (green)  
74 and Stop trials (red) in the above referred epoch T. Most SAs display a clear difference between correct

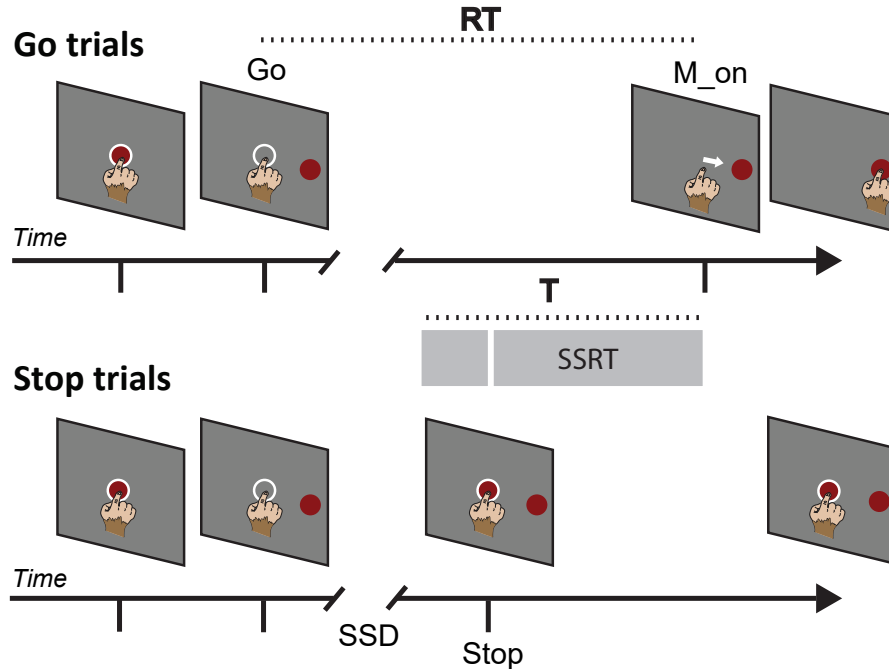


**Figure 1.** Sequence of behavioural event characterizing the task. Go and Stop trials were randomly intermixed during each session. The epoch (T) of neural analysis is shown as a grey bar. For Go trials, the SSRT marks the time, before movement execution, that would have corresponded to the presentation of the Stop signal. For correct Stop trials SSRT marks the time, after the Stop signal presentation, that would have corresponded to the movement execution. RT, reaction time; SSD, stop signal delay; SSRT, stop signal reaction time.

75 Stop trial and Go trials after the Stop signal (vertical red line), i.e., during the session-specific SSRT,  
76 reflecting the active participation of PMd in the decision to generate or inhibit reaching movements.  
77 Several features are observable. For example, the time of divergence between the two activities for the  
78 different channels was highly variable. Moreover, in some cases (e.g., channels 25 and 43) the observed  
79 pattern was completely opposite (more intense activity in Stop trials than in Go trials). A similar overall  
80 picture was evident in all recorded sessions. In short, the various modules seem to contribute to the control  
81 exerted on the movement to be performed by PMd in a very heterogeneous way. Of relevance, from  
82 these considerations nothing can be inferred about the information transfer and the functional relationship  
83 between different modules.

84 To investigate directed information transfer between the network modules we used Transfer Entropy  
85 (TE), a well-established model-free information theoretic method<sup>22</sup>. In a given epoch TE can detect  
86 asymmetric information flows among the modules, and hence it allows defining modules acting as drivers  
87 (or sources) or targets of information transfer (see Materials and Methods for further details). To evaluate  
88 whether the different behavioural conditions of the task were characterized by different local information  
89 dynamics we computed TE between trial-averaged time series (i.e., in the epoch T) of SA separately for  
90 Go and correct Stop trials.

91 We found that some of the modules were drivers in both Go and Stop conditions (**Common\_drivers**);  
92 others were drivers in one behavioural condition only (**Go\_drivers** and **Stop\_drivers**); others were never  
93 drivers and just targets of information flow (**Targets**) (see Table 2; see Materials and methods for further

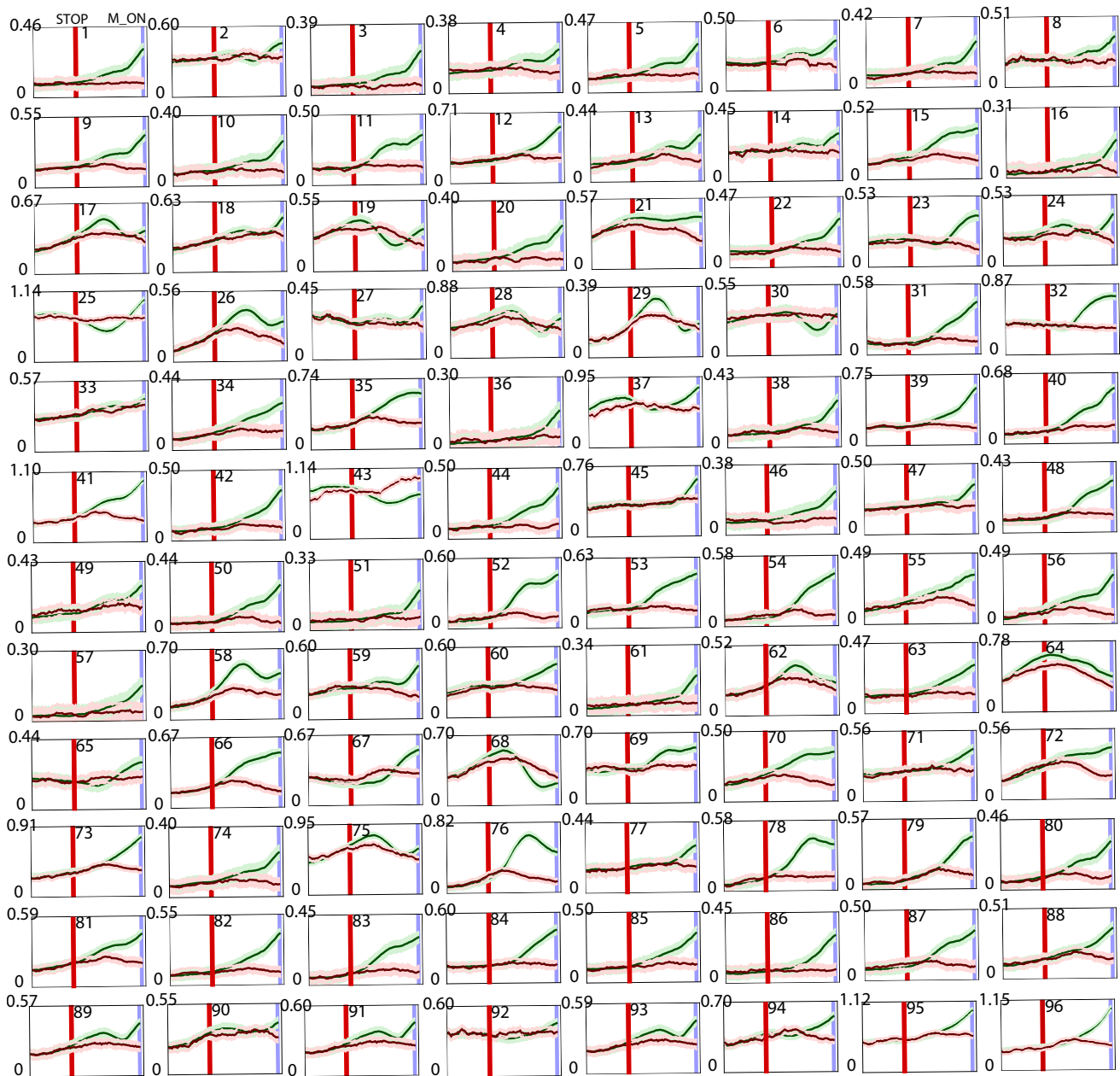


**Figure 2.** Neuronal modulation in the two behavioural conditions for all channels of a typical recording session. Green traces show the average activity during Go trials aligned to Movement onset (rightmost part of the plot). Red traces show the average activity during correct Stop trials aligned to the Stop signal presentation (red vertical line). The epoch between the stop signal and the movement onset is the session SSRT.

Behavioural Results						
Monkey P						
<i>S</i>	$\overline{RT}_{Go}$	$\overline{RT}_{Wr}$	$\overline{SSD}$	<i>SSRT</i>	$P_{inhibit}$	<i>p-value</i>
1	590 ms	559 ms	273 ms	317 ms	0.52	$p < 0.05$
2	584 ms	564 ms	277 ms	307 ms	0.50	$p < 0.05$
3	575 ms	503 ms	293 ms	282 ms	0.69	$p < 0.05$
4	618 ms	592 ms	335 ms	283 ms	0.52	$p < 0.01$
5	868 ms	549 ms	675 ms	193 ms	0.58	$p < 0.01$
6	572 ms	540 ms	293 ms	279 ms	0.50	$p < 0.05$
7	643 ms	622 ms	382 ms	261 ms	0.51	$p < 0.05$
8	600 ms	568 ms	340 ms	260 ms	0.48	$p < 0.01$
9	656 ms	641 ms	445 ms	211 ms	0.37	$p < 0.01$
10	788 ms	753 ms	528 ms	260 ms	0.54	$p < 0.01$
11	674 ms	619 ms	418 ms	256 ms	0.56	$p < 0.01$
12	765 ms	721 ms	504 ms	261 ms	0.51	$p < 0.01$
Monkey C						
1	598 ms	523 ms	322 ms	276 ms	0.57	$p < 0.01$
2	539 ms	460 ms	382 ms	157 ms	0.65	$p < 0.05$
3	561 ms	522 ms	318 ms	243 ms	0.58	$p < 0.01$
4	673 ms	625 ms	424 ms	249 ms	0.60	$p < 0.05$
5	636 ms	608 ms	396 ms	240 ms	0.55	$p < 0.05$
6	575 ms	533 ms	292 ms	283 ms	0.42	$p < 0.01$
7	667 ms	620 ms	383 ms	284 ms	0.60	$p < 0.05$
8	688 ms	672 ms	413 ms	275 ms	0.43	$p < 0.05$
9	688 ms	657 ms	402 ms	286 ms	0.60	$p < 0.01$

**Table 1. Behavioural results.** *S*, index of the recording session.  $\overline{RT}_{Go}$ , mean reaction time of Go trials.  $\overline{RT}_{Wr}$ , mean reaction time of wrong-stop trials.  $\overline{SSD}$ , mean SSD of Stop trials. *SSRT*, Stop Signal Reaction Time.  $P_{inhibit}$  inhibition probability. The *p-values* result from the independence (Kolmogorov-Smirnov test between  $\overline{RT}_{Go}$  and  $\overline{RT}_{Wr}$ ).

94 details). Figure 3 shows, for illustrative purpose only, a schematic of a network organized as observed.  
 95 The presence of different classes straightforwardly showed that the intrinsic composition of the PMd  
 96 information network is heterogeneous, with some of the modules operating as drivers only in relation  
 97 to a specific behavioral outcome (moving vs withholding). This hinted that the network configuration  
 98 underlying information transmission changes according to the specific decision and behavioural output.

99 **Neuronal activity classes are hierarchically organized. Common\_drivers act as main**  
 100 **hubs for information transmission within PMd. Go/Stop\_drivers act as hubs only in rela-**  
 101 **tion to specific behavioural conditions**

102 To better understand the role of the identified classes (i.e, Common, Go, Stop drivers and Targets) in the  
 103 PMd network we investigated the topology of information transmission for each recording session and  
 104 behavioural condition. In this framework each entry (module) of the TE matrix is interpreted as a node of



Classes Composition	
Monkey P $N = 96$	
Class	$\mu \pm SD$
Go_drivers	$6.46 \pm 2.90$
Stop_drivers	$13.71 \pm 3.22$
Common_drivers	$8.62 \pm 3.60$
Targets	$67.20 \pm 4.88$
Monkey C $N = 79$	
Class	$\mu \pm SD$
Go_drivers	$6.78 \pm 3.93$
Stop_drivers	$9.56 \pm 3.78$
Common_drivers	$7.00 \pm 2.06$
Targets	$55.70 \pm 5.29$

**Table 2. Classes composition.** For each monkey the composition of classes averaged over recording sessions is reported. Composition is expressed as the average number of nodes ( $\mu$ ) belonging to each class. SD, standard deviation.  $N$ , the number of channels available.

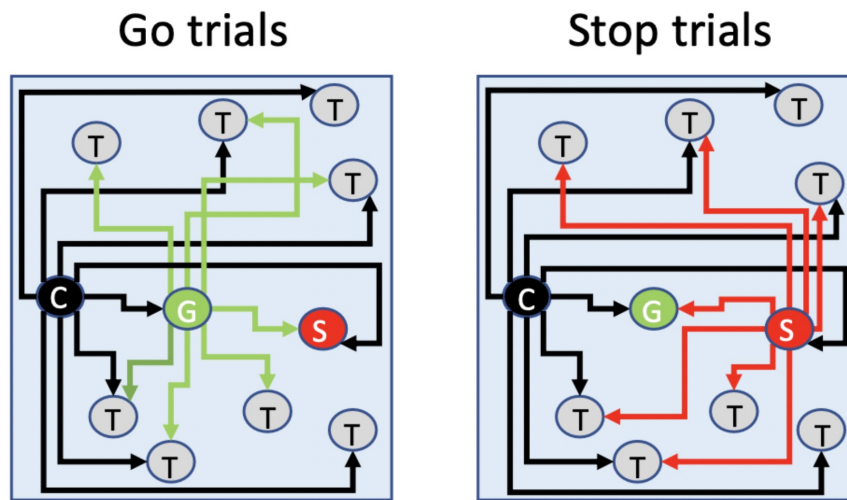


**Figure 3.** Schematic representation of a network organized with three different classes of drivers nodes (Common\_drivers, black; Go\_drivers green; Stop\_drivers red) and targets (grey nodes). The role of the Go\_drivers and Stop\_drivers changes in relation to the condition (Go trials vs Stop trials).

105 the network, and each link (or connection) is the information exchanged between nodes (see Materials  
 106 and methods for further details). To quantify the topology of information transmissions we resorted to  
 107 different graph-based measures.

108 We first computed the **vertex degree** (VD), i.e. the number of connections per module. A high value of  
 109 the VD indicates that the module is connected with many others. The opposite holds for a low value of  
 110 VD. Thanks to the asymmetry of TE, which defines drivers and targets, for each module it is possible to  
 111 distinguish between the information directed towards other modules ( $VD_{out}$ ) and the information incoming

112 from other modules ( $VD_{in}$ ). We examined the  $VD_{out}$  and the  $VD_{in}$  distributions for each recording  
113 session of both monkeys and we observed that only  $VD_{out}$  distributions were fat-tailed (see supplementary  
114 Figure S1). The high values of  $VD_{out}$  associated to the tails indicate modules with a number of outwards  
115 connections that greatly exceed the average value (see Materials and Methods). These modules are network  
116 hubs<sup>23</sup>. The VD values, together with the direction of information flow detected by TE, allow better  
117 defining a hierarchy of information transmission among modules. Indeed, given a driver and a target the  
118 driver is always located hierarchically above the target (see Figure 8 in the Materials and Methods section)  
119 . Moreover, the existence of hubs means that a few modules determine the state of many others, and hence  
120 the global configuration of the network. Fig 4 shows the topology of PMd network in both behavioural  
121 conditions for an example session of Monkey P (examples from other sessions for both monkeys are  
122 shown in supplementary Figure S2). Each module is assigned to a class as previously obtained from  
123 the analysis of the TE distributions and coloured accordingly. The size of the dots here used to identify  
124 each module (node) reflects its  $VD_{out}$  value, i.e. the number of modules on which it acts as a driver. The  
125 arrow for each connection indicates the direction (in/out) for the information path. In Go trials (top) the  
126 topology documented a more centralized (in terms of  $VD_{out}$ ) organization (star-like topology) compared  
127 to the Stop trials (bottom), confirming previous observations<sup>18</sup>. Indeed, in a recent study on correlation  
128 networks during the same task we showed that the presence of a star-like topology in the PMd network  
129 is the hallmark of the incoming movement. Here, by adding the insights provided by the TE analysis,  
130 the emerging picture is of a network changing not only in the overall organization but also in the role of  
131 the components. To this extent, Fig 4 shows that Stop\_drivers emerge as important nodes in information  
132 spreading in Stop trials only.

133 Figure 5 (top panels) shows, for all sessions, that the Common\_drivers exhibited the highest values of  
134  $VD_{out}$  (See Table 3 for the corresponding statistics) compared to other classes in both Go and correct Stop  
135 trials, thus resulting as the principal information-spreaders hubs across different behavioural conditions.  
136 Therefore, Common\_drivers are located at the highest hierarchical level in the network as they regulate  
137 information transfer whatever decision, moving or stopping, is taken (see also next paragraph). Conversely,  
138 Go\_drivers and Stop\_drivers displayed a different role (different  $VD_{out}$  values) in Go and Stop trials,  
139 suggesting that the hierarchical organization of the network changes in relation to the motor decision  
140 process. Indeed, Stop\_drivers are never hubs in Go trials and Go\_drivers are never hubs in Stop trials.  
141 As a further measure of the organization of the PMd network we used **betweenness centrality**<sup>24,25</sup> (BC).  
142 BC quantifies the influence that a given node has over the flow of information between other nodes.  
143 Therefore, it gives a measure of how a node controls communications in a network. BC is computed as  
144 the fraction of shortest paths between all nodes in the network that pass through a given node. Since we  
145 are dealing with an information network, we used BC to quantify the capability of each node to mediate  
146 and route the information traffic. An high BC value indicates that a node strongly mediates information  
147 flow because it lies on a considerable fraction of shortest paths. Hence, nodes with high BC values are  
148 topological central nodes. As reported in Fig 5 (panel A, bottom) and in Table 3, we found higher BC  
149 values during correct Stop trials compared to Go trials meaning that during correct Stop trials information  
150 traverses an higher number of shortest paths. This implies that a shift toward a less direct (and hence less  
151 centralized in terms of  $VD_{out}$ ) communication between nodes occurs during Stop trials only; information  
152 is detoured through more shortest paths resulting in a more distributed and widespread transmission. An  
153 intuition can be gained by noticing the arrangement of the graphs during correct Stop trials which results  
154 more “expanded” than the optimal star-like configuration of Go trials (see Figure 4). Analogously to  
155 what found during the analysis of  $VD_{out}$ , Go\_drivers and Stop\_drivers (green and red dots in Fig 4)  
156 displayed a different role (different BC values) in Go and correct Stop trials respectively, confirming  
157 the specificity of these classes in relation to the behavioural conditions. The values of BC found for the

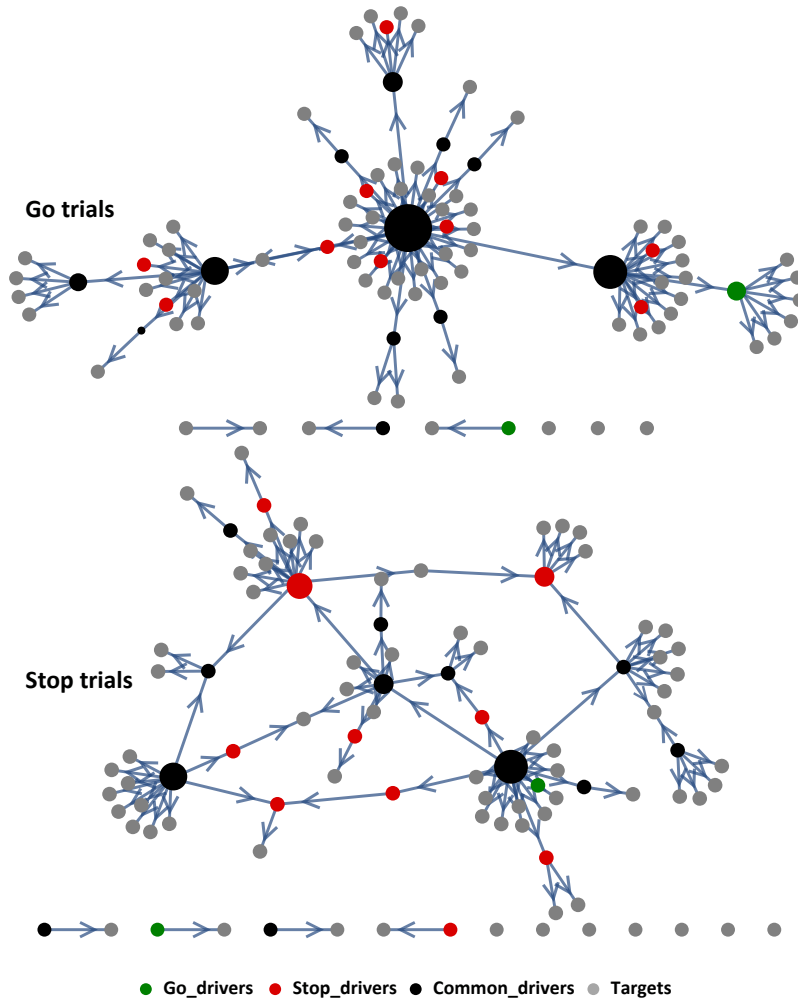


**Figure 4. Information network of Go and Stop trials** for data in Figure 2. Each node is coded accordingly to the corresponding class (see legend in the lower part of the figure). The size of the nodes is scaled according to the corresponding  $VD_{out}$ , thus bigger nodes are the information-spreaders hubs (see text for details).

158 Common\_drivers (black dots in Fig.4) during both behavioural conditions corroborate what was found  
159 via the  $VD_{out}$  analysis: in the PMd information network they manage and distribute the information flow.  
160 Moreover, during movement inhibition the actors that collaborate the most with the Common\_drivers in  
161 rerouting and reverberating communications are the Stop\_drivers.

162

163 To have a compact view of the overall differences between the  $VD_{out}$  and BC measures across  
164 behavioural conditions we computed a summarising index for both topological measures named **central-**  
165 **ization index**  $C^{24,25}$ .  $C$  is the total average difference between the highest value of the centrality measure  
166 inspected ( $VD_{out}$  and BC in our case) and the values assumed by all the other nodes. High values of  $C$   
167 indicate that nodes with high centralities with respect to the other nodes in the network exist.  $C$  is an  
168 easy and intuitive way to compare the overall organization of networks in terms of centrality measures  
169 (see Materials and methods). We computed  $C$  for both measures for each recording session and then  
170 we averaged over sessions. Panel A of Figure 6 reports the average centralization indexes compared



171 between behavioural conditions for both animals (results from each sessions are reported in panel A of  
172 supplementary figure S3). As expected,  $C$  of  $VD_{out}$  ( $C_{vd}$ ) decreases from Go to correct Stop trials while  
173 the opposite holds for  $C$  of  $BC$  ( $C_{bc}$ ). This confirms, at the overall level, how information processing is  
174 based on different topologies during the two behavioural conditions.

175  
176 We then calculated the **total information**  $TE_{total}$  processed during Go trials and correct Stop trials  
177 (Figure 6, panel B and supplementary figure S3 panel B). We found that during correct stop trials less  
178 information was processed compared to Go trials. This means that the overall changes in the topological  
179 arrangement of the the PMd network correspond to overall changes in the amount of information exchanged.  
180 More specifically, the increase in BC during correct Stop trials is accompanied by a reduction in the total  
181 amount of information elaborated.

182 To sum up, we demonstrated with the used graph measures that classes are hierarchically organized in  
183 PMd during movement planning and suppression and that information is processed differently and to a  
184 lesser extent during correct stop trials compared to Go trials. Results revealed the Common\_drivers as the  
185 most topological central nodes in the network with the Go\_drivers and the Stop\_drivers playing a crucial  
186 supporting role in the processing of information during movement planning and inhibition respectively.

## 187 **Different interactions among neuronal classes characterize behavioural conditions**

188 To summarize the interactions among classes we computed the average amount of information exchanged  
189 between the four classes during both behavioural conditions. To this end, we constructed a 4x4 matrix  
190 ( $I$ ) whose generic entry is given by equation 7. We then represented the **matrix I** as a network in which  
191 each node is now a class. This makes possible to have a compact picture of the differences between  
192 Go and correct Stop trials in terms of interactions between classes. We calculated  $I$  (see Material and  
193 Methods for details) for both behavioural conditions of each recording session and we then averaged  
194 over sessions; results are shown in Figure 7 (see also Table 4). The Common\_drivers were confirmed  
195 to be part of the high order class in the network since they transmit to other classes without receiving.  
196 Indeed, even when the Go\_drivers and Stop\_drivers emit information on their own, they receive from the  
197 Common\_drivers. This means that the first ones are hierarchically located at a lower level. Moreover, the  
198 extent of communication of the Common\_drivers with the Targets is significantly greater than that of the  
199 Go\_drivers and Stop\_drivers (see Table 4). This implies that the Common\_drivers determine the global  
200 state of the network with Go\_drivers and Stop\_drivers playing a supporting role. It is worth noticing that  
201 the specificity of Go\_drivers and Stop\_drivers is confirmed by the direction of their interactions during  
202 behavioural conditions. In fact, during Go trials the Go\_drivers transmit to the Stop\_drivers helping  
203 the Common\_drivers in the control while the opposite happens during correct Stop trials. The amount  
204 of information that the Common\_drivers distribute in the network diminishes from Go to correct Stop  
205 trials. This complement and helps to better understand what said in the previous section: patterns of  
206 information transfer change from Go to correct Stop trials, with the network undergoing a less direct  
207 configuration during the latter due to an increased number of shortest paths between the nodes. Network  
208 interactions are consistent across recording sessions for both monkeys (see Table 4). Common\_drivers are  
209 always hierarchically above the other classes and orchestrate communication: they transmit information to  
210 other classes in both behavioural conditions without receiving information from the other classes of the  
211 analysed PMd network. Moreover, during Go trials Go\_drivers participate transmitting to the Targets as  
212 the Stop\_drivers do during correct Stop trials.

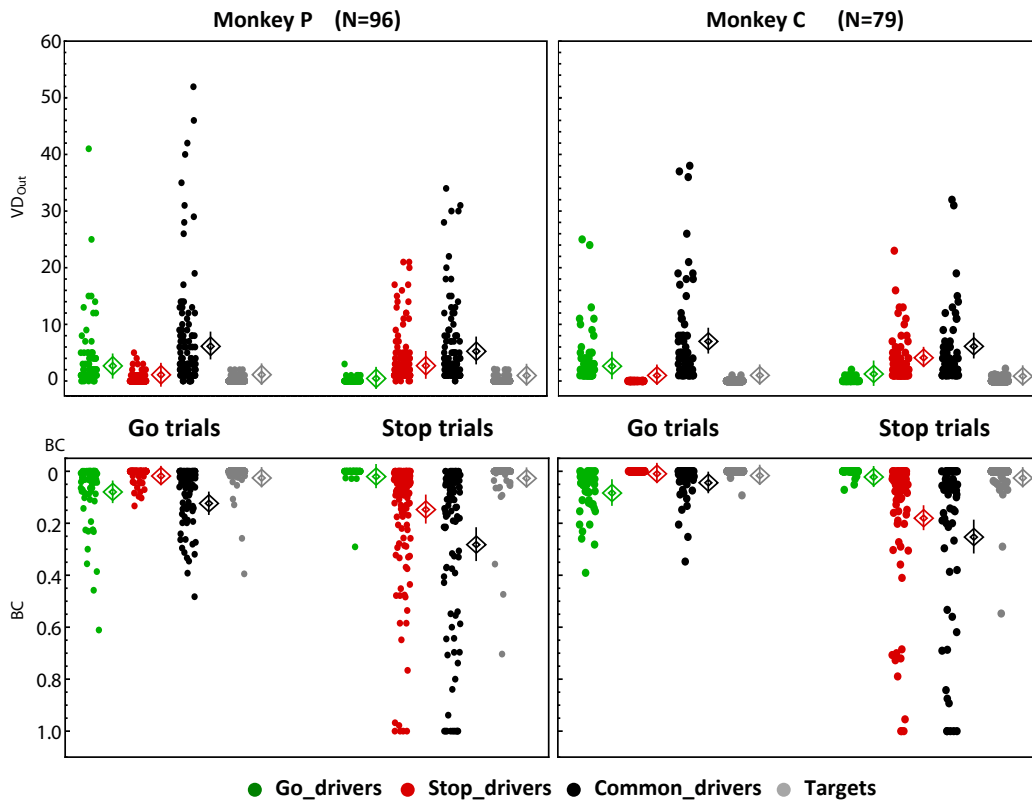


**Figure 5. Measures for topology of information transmission.** **Top panels:**  $VD_{out}$  values compared across behavioural conditions for all recording session. The Common class (black points) shows the highest values of  $VD_{out}$  compared to other classes in both behavioural conditions (for both monkeys, all adjusted p-values  $Qs < 0.01$ ). Go\_drivers and Stop\_drivers show the second highest  $VD_{out}$  values during Go (for both monkeys all  $Qs < 0.01$ ) and correct Stop (for both monkeys all  $Qs < 0.01$ ) trials respectively. **Lower panels:** BC values compared across behavioural conditions for all recording session (here scaled for simplicity to the maximum value of each session so to have values in the range [0,1]). Go\_drivers and Stop\_drivers classes have, together with the Common, the highest values of BC during Go and correct stop trials respectively (for both monkeys all  $Qs < 0.01$ ). The Stop\_driver class is the one with the greatest increase ( $\Delta_{Stop-Go}$ ) in BC passing from Go to correct Stop trials (for both monkeys all  $Qs < 0.01$ ). Colours reflect the neuronal classes as in Figure 4. Means and standard errors are indicated by the diamonds and related lines. Statistics is based on the adjusted p-value (Q) obtained from Kolmogorov Smirnov tests and false discovery rate (FDR) correction. See Table 3 for the details.

## 213 Discussion

214 In this work we investigated the patterns of information transfer in a localized cortical network (the PMd)  
 215 directly involved in movement decision-making. We used a combined Transfer Entropy and graph-based  
 216 approach to analyse simultaneously recorded SAs (from up to 96 channels). Our results contribute to  
 217 move forward the knowledge on the neural basis of action decision-making at different levels.

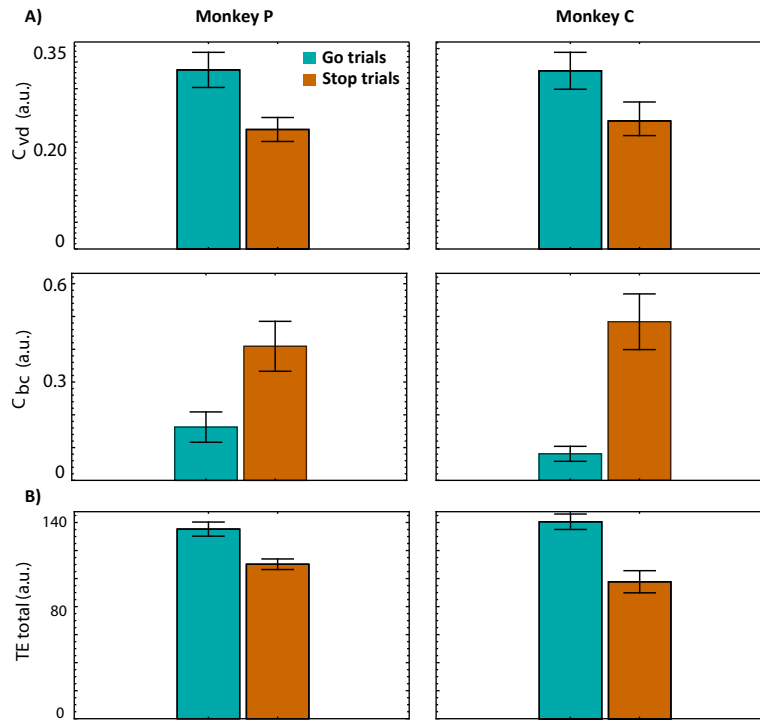


**Figure 6. Overall network comparison between behavioural conditions. Panel A** The overall centralization index  $C$  for both  $VD_{out}$  ( $C_{vd}$ ) and BC ( $C_{bc}$ ) measures averaged over recording sessions and compared between behavioural conditions for both monkeys.  $C$  gives an overall topological comparison of the information network compared between behavioural conditions. **Panel B** Total information processed averaged over recording sessions compared between behavioural conditions. Cyan: Go trials. Orange: correct Stop trials. Error bars are given by the standard error of the mean.

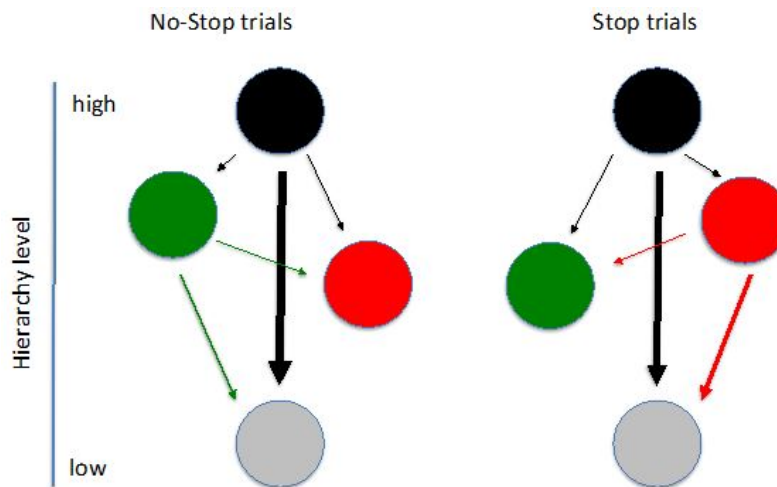


**Figure 7. Network representation of interactions between classes in the two behavioural conditions:** Colours codes for the classes are the same of the previous figures. Uncertainties are obtained via error propagation (see materials and methods).

## 218 **A topological approach to the organization and spreading of local information in a decision-** 219 **making task**

220 The first level of advancement is methodological: we employed a graph-based approach combined with  
221 information theoretic measures (specifically multivariate Transfer Entropy (TE)) to investigate neuronal  
222 interactions underlying motor control. Although TE is growing in popularity in modern neuroscience its  
223 application to invasive electrophysiological data has been so far very limited and restricted to either single  
224 neurons or in vitro<sup>26–28</sup> and in silico studies<sup>29</sup>. Shimono and Beggs<sup>26</sup> used it at the single neuron level to  
225 investigate the structure at different scale of rodent somatosensory cortex<sup>26,30</sup>. Timme and colleagues<sup>31</sup>  
226 recorded the activity of hundreds of neurons in cortico-hippocampal slice cultures and used TE to study the  
227 information transfer changes therein. An early contribution to this research topic is from Gerhard et al<sup>32</sup>,  
228 that inspected the topology of spike trains recordings from the visual system of a rhesus monkey during a  
229 fixation task. However, the authors used a different approach to measure directed connectivity. Another  
230 contribution comes from the work of Honey<sup>33</sup>, that investigated a large-scale interregional anatomical  
231 network of the macaque cortex through transfer entropy. An attempt to study voluntary action control  
232 through analysis of directed connectivity was made by Jahfari and colleagues<sup>34</sup> but on human MRI data.  
233 Hence, to the best of our knowledge, this report is one of the very few studies that uses graph theory to  
234 analyse the information transfer network of a specific cortical area at the mesoscale level in vivo and  
235 during a behavioural task. The level of description here obtained is more detailed compared to previous  
236 works. Indeed, we were able to specify how the decision on whether to move or to stop is implemented  
237 in PMd at the population level and who are the (key) players that manage information transmission.  
238 Notably, in our framework neither any a priori assumption nor a specific neural modelling technique  
239 was needed. Our completely data-driven approach, in addition to complement the most recent models  
240 for motor generation and suppression<sup>35,36</sup>, permits to overcome their main limitation which resides in  
241 the requirement of many biophysical parameters to be tweaked and tuned before fitting with acceptable  
242 accuracy the experimental data. Although is still not largely used in behavioural neurophysiological  
243 studies at the small and mesoscale, a graph-based conceptualization of neural interactions, united with  
244 information theoretic measures, can be very profitable also compared to other common approaches based  
245 on analysis of covariance between neurons or mesoscopic signals<sup>7,37–40</sup> and should be exploited more. In  
246 fact, these methods are not straightforward in distinguishing the specific contributions of single neurons  
247 (or discrete populations of neurons) to the topology of network dynamics, which is indeed the strength of  
248 our strategy. On one hand this range of methods allows for a fine temporal description of neural variability  
249 but on the other, due to their nature, are neither capable to describe the information flow between neuronal  
250 actors nor to provide quantitative insights on the topology of network connections and their hierarchical  
251 organization. Without this all spectrum of details the computational strategy underlying motor control  
252 (and neural circuitry computation in general) would be yet elusive. Recently, some authors have have  
253 started to follow the joint information theory-complex networks approach but for now, to the best of our  
254 knowledge, only on cortico-hippocampal<sup>31</sup>, somatosensory cortex slice cultures<sup>26</sup> and anesthesiological<sup>41</sup>  
255 data. It is known that to fully understand the neural mechanisms behind motor control future research  
256 should focus on cortico-cortical and cortico-subcortical interactions through simultaneous recordings. In  
257 this scenario a topological information-based approach would be unquestionably necessary to gain an  
258 overall view and elicit detailed insights.

## 259 **A race with more than two horses is in act in PMd when movements are successfully** 260 **suppressed**

261 The second level of advancement concerns the novelty of our results compared to other studies, especially  
262 those that focused on the possible interaction among different classes of neurons during motor decision. We

263 found, in the characterized PMd network, that neuronal activities could be organized around four different  
264 classes and that they actively participate, even with different roles, both in movements execution and  
265 cancellation. This constitutes a step forward in the conceptualization of the neural processes at the base of  
266 movement generation since all the widely accepted models for inhibitory control of movements<sup>35,36,42–45</sup>  
267 are deduced from the analysis of single unit firing rates and are based on the interaction of only two modules  
268 (or class of neurons) often reported as Go and Stop units. We instead demonstrated that information is  
269 hierarchically transferred between more than two actors with the Common class nodes acting as network  
270 hubs. This reflects the existence of a high-order complexity in functional communications and organization  
271 at the population level, even in small portions of the cortex, during behavioural control regardless of  
272 which the nature of neurons in each class might be (i.e. excitatory or inhibitory neurons etc.. ). Indeed,  
273 based only on the information emitted by each local module we managed to isolate both condition-specific  
274 and nonspecific neuronal classes. It is worth stressing that we drew our conclusion on the heterogeneity  
275 of neuronal classes in a completely data-driven and model-free fashion, and this strengthens the results.  
276 Additionally, we showed the details of how this transfer occurs at the population level and to what  
277 extent it depends on behavioural conditions. Our picture integrates the current view because besides  
278 specific classes involved in the generation (Go\_drivers) and inhibition (Stop\_drivers) of movements, it  
279 establishes the existence of a high order class (Common\_drivers) not proposed in other works. This  
280 highlights, for the first time at the mesoscale resolution, the existence of a fine-grained organization of  
281 neural assemblies at the population level that handle intra-area information flow. It is worth pointing  
282 out that usual methods of studying neural activity profiles are not sufficient to infer all aspects of such  
283 architecture. The Common\_drivers are higher in hierarchy with respect to the others for two reasons.  
284 The first is because they transmit information to the whole network without receiving from inside the  
285 same network. From the information theoretic point of view this indeed means that the state of the other  
286 classes can be better predicted by the state of the Common compared to that of the other classes. Thus,  
287 the state of the whole local network depends on the state of the Common\_drivers. The second one is  
288 topological, being the Common\_drivers the most widespread hubs across behavioural conditions. The  
289 found subdivision in classes, the presence of hubs and topological central nodes deputed to the rerouting  
290 of communications reveal that the cortical information dynamics behind motor control is extremely rich  
291 and cannot be entirely explained by the current proposed models. The found topology also implies that  
292 the presence of high-degree nodes is a constituent feature of neural processing in a cortical network  
293 directly involved in cognitive control, as is the PMd. This is consistent with our previous study<sup>18</sup> in  
294 which we showed how the functional PMd network organization differs between movement generation  
295 and inhibition in terms of hierarchy and centrality of nodes. It is also in agreement with other works that  
296 found fat-tailed degree distributions in silico<sup>46</sup>, in cortical and hippocampal in vitro networks<sup>26,47–50</sup>, in  
297 vivo<sup>51</sup> and structural networks<sup>33</sup>. We found that the arrangement of the PMd information network depends  
298 on the behavioural condition, passing from a centralized star-like state during movement planning to a  
299 different one during movement inhibition characterized by high values of Betweenness Centrality and  
300 a minor transfer of information. We interpret this reorganization as the execution in the local network  
301 of a command originating from other regions. Indeed, as known, the PMd is part of a larger network  
302 subserving motor control based on frontal, parietal, subcortical and spinal structures. Is reasonable to  
303 think that during Go trials the hubs serve to convey the command to move to other (and possibly lower)  
304 cortical, subcortical, and spinal circuits that will eventually promote muscle activation. In this picture, the  
305 state observed during correct stop trials could reflect the PMd collective reaction to the incoming inhibitory  
306 thalamic input that prevents the execution of the programmed movement. In this scenario the volition  
307 to inhibit is locally implemented as ‘the attenuation of the movement state’, which seems convenient and easy  
308 to implement at the network level detouring information flow through an higher number of shortest paths



309 between nodes and decreasing the amount of information involved. Future studies will be necessary to  
310 investigate to whom the hubs project to.

311 One weakness of this study is that we cannot account for the information dynamic between PMd and  
312 other structures of the reaching network. Therefore, additional research will be needed to unambiguously  
313 clarify these interactions. Lo et al.<sup>36</sup> also introduced a certain degree of hierarchical organization in the  
314 form of a top-down control regulating the activation of the Go and Stop unit. However, as also stated in  
315 Schall et al.<sup>44</sup>, the control unit embodied in their model resembled an external homunculus endowed with  
316 the ability to tune the parameters to appropriately obtain the desired results. This marks a considerable  
317 difference with our report, in which, since our approach is completely data-driven, we did not need to  
318 adjust any external modelling unit to obtain the results.

319 Conversely, we used it conceptually to contextualize our results in a wider circuitry frame. Lastly, our  
320 findings clearly show that hierarchical control is not only external but is also implemented locally by a  
321 specific neuronal class (the Common\_drivers) over the others. Through the years, much evidence has  
322 been brought to support the idea that the brain is hierarchically organized both globally and locally on  
323 a spatial<sup>18,52-63</sup> (for a detailed review see Hilgetag et al., 2020<sup>64</sup>) and temporal scale<sup>65-70</sup>. As far as we  
324 know, this is the first work that deeply investigates the local hierarchy of a single cortical area known to  
325 have a crucial role in the motor system. These conclusions suggest that the collective network organization  
326 found in this work represents the neural implementation for the voluntary motor control at the PMd level.

## 327 **Materials and methods**

### 328 **Subjects**

329 Two male rhesus macaque monkeys (*Macaca mulatta*, Monkeys P and C), weighing 9 and 9.5 kg,  
330 respectively, were used. Animal care, housing, surgical procedures and experiments conformed to  
331 European (Directive 86/609/ECC and 2010/63/UE) and Italian (D.L. 116/92 and D.L. 26/2014) laws and  
332 were approved by the Italian Ministry of Health. Monkeys were pair-housed with cage enrichment. They  
333 were fed daily with standard primate chow that was supplemented with nuts and fresh fruits if necessary.  
334 During recording days, the monkeys received their daily water supply during the experiments.

### 335 **Apparatus and task**

336 The monkeys were seated in front of a black isoluminant background ( $< 0.1\text{cd}/\text{m}^2$ ) of a 17-inch  
337 touchscreen monitor (LCD, 800 x 600 resolution), inside a darkened, acoustic-insulated room. A non-  
338 commercial software package, CORTEX (<http://www.nimh.gov.it>), was used to control the presentation  
339 of the stimuli and the behavioural responses. Fig. 1 shows the scheme of the general task: a reaching  
340 countermanding task (Mirabella et al., 2011). Each trial started with the appearance of a central target  
341 (CT) (red circle, diameter 1.9 cm). The monkeys had to reach and hold the CT. After a variable holding  
342 time (400–900 ms, 100-ms increments) a peripheral target (PT) (red circle, diameter 1.9 cm) appeared  
343 randomly in one of two possible locations (right/left) and the CT disappeared (Go signal). In no-stop  
344 trials, after the Go signal the subjects had to reach and hold the PT for a variable time (400-800 ms, 100ms  
345 increments) to receive juice. Reaction times (RTs) were defined as the time between the presentation of the  
346 Go signal and the onset of the hand movement. In Stop signal trials, the sequence of events was the same  
347 until the Go signal. Then, after a variable delay (Stop signal delay, SSD), the CT reappeared (Stop signal)  
348 and the monkeys had to hold the CT until the end of the trial (800–1000 ms) to receive the reward (correct  
349 stop trial). Conversely, removing the hand after the Stop signal constituted a wrong response (wrong stop  
350 trial). The same amount of juice was delivered for correct stop and correct no-stop trials. The intertrial  
351 interval was set to 800 ms. Stop trials represented the 25% of all trials in each recording session. To

352 establish the duration of the SSDs, a staircase tracking procedure was employed. If the monkey succeeded  
353 in withholding the response, the SSD increased by one step (100 ms) in the subsequent Stop signal trial.  
354 Conversely, if the subject failed, the SSD decreased by one step.

## 355 Behavioural considerations

356 In the countermanding task is of crucial importance the identification of the neuronal signature of the  
357 movement execution and its time of occurrence. The task makes possible to calculate a behavioural  
358 measure that it is broadly considered an index of efficiency in movement suppression: the stop signal  
359 reaction time or SSRT. To estimate SSRT the race model<sup>71</sup> is the accepted paradigm. This model describes  
360 the behaviour in the stop trials as the result of two stochastic processes racing toward a threshold: the  
361 GO process triggered by the onset of the Go signal, which duration is represented by the RT, and the  
362 STOP process triggered by the onset of the Stop signal, which duration must be calculated. When the GO  
363 process wins the race the movement is generated (wrong Stop trials), alternatively it is withheld (correct  
364 Stop trials). The race model allows to estimate the SSRT by considering the duration of the GO process,  
365 the probability to respond, and the SSDs. However, to make the race model applicable to study response  
366 inhibition, a central assumption must be satisfied: the GO process in the stop trials must be the same  
367 as in the go trials (independence assumption). Indeed, the RTs that are employed to estimate the SSRT  
368 are obtained from the Go trials distributions. To broadly validate this assumption, wrong Stop trials RTs  
369 must result shorter than the correct Go trials RT<sup>71</sup> (see Table 1). To estimate the SSRT we employed the  
370 integration method because it has been proven to be the most reliable<sup>72</sup>. It assumes that the finishing time  
371 of the Stop process corresponds to the  $n$ th go RT, where  $n$  results from the multiplication of the ordered  
372 Go RTs distribution by the overall probability of responding  $p(\text{respond})$ . The SSRT is then obtained by  
373 subtracting the average SSD from the  $n$ th Go RT. The SSRT can also be considered the lead time that is  
374 required to inhibit a movement, or, simply, the time that precedes the start of a movement when a Stop  
375 signal, if presented, halts the generation of the same movement approximately 50% of the time. If the  
376 Stop signal is presented after this time, it will be less effective, because the neuronal phenomena that lead  
377 to the movement generation will have already started. If the Stop signal is presented well before this time,  
378 it will be more effective in halting the movement. Consequently, the neuronal activity that is related to  
379 movement generation must occur before movement onset around the time that is defined by the SSRT.

380 The aim of our study was to compare conditions in which a movement was planned and then generated  
381 (Go trials) to those in which a movement was planned and then inhibited (correct Stop trials). To correctly  
382 compare the two behavioural conditions, a time window  $T$  equivalent for both trial types must be defined.  
383 Assuming that a time  $t_{go}$  ms before movement onset is chosen and an SSRT of  $t_{ssrt}$  ms is estimated,  $T$  in  
384 correct Stop trials is given by  $T = [- (t_{go} - t_{ssrt}), + t_{ssrt}]$  ms with respect to the Stop signal presentation.  
385 Notice that  $T$  accounts for any time difference with respect to the SSRT trough the term  $(t_{go} - t_{ssrt})$ .

386 Behavioural parameters for the recording sessions of the two monkeys analyzed in this study are  
387 reported in Table 1.

## 388 Extraction and processing of neuronal data

389 A multielectrode array (Blackrock Microsystems, Salt Lake City) with 96 electrodes (spacing 0.4 mm) was  
390 surgically implanted in the left dorsal premotor cortex (PMd; arcuate sulcus and pre-central dimple used  
391 as references after opening of the dura) to acquire unfiltered electric field potentials (UFP; i.e., the raw  
392 signal), sampled at 24.4 kHz (Tucker Davis Technologies, Alachua, FL). As a measure of neuronal activity  
393 at the population level, SA was extracted offline from the raw signal, as in Mattia et al.<sup>7</sup>, by computing the  
394 time-varying power spectra  $P(\omega, t)$  from the short-time Fourier transform of the signal in 5-ms sliding  
395 windows. Relative spectra  $R(\omega, t)$  were then obtained normalizing  $P(\omega, t)$  by their average  $P_{\text{ref}}(\omega)$  across

396 a fixed window (30 minutes) for the entire recording. Thus, the average  $R(\omega, t)$  across the  $\omega/2\pi$  band  
 397  $[0.2, 1.5]$  kHz represent the spectral estimated SAs. As better detailed in Mattia et al.<sup>7</sup>, such estimate relies  
 398 on two hypotheses. The first is that high  $\omega$  components of the raw signal result from the convolution of  
 399 firing rates  $v(t)$  of neurons that are close to the electrode tip with a stereotypical single-unit waveform.  
 400 The Fourier transform  $K(\omega)$  of such an unknown waveform is canceled out in  $R(\omega, t)$ , which is therefore  
 401 a good approximation of the ratio of firing rate spectra  $|v(\omega, t)|^2 / |v(\omega, t)|_{\text{ref}}^2$ . The second hypothesis is  
 402 that high  $\omega$  power  $|v(\omega, t)|^2$  is proportional to the firing rate  $v(t)$  itself<sup>73</sup>, such that our SA estimate is  
 403 proportional to  $v(t)$ . As a last step, logarithmically scaled SAs were smoothed by a moving average (40  
 404 ms sliding window, 5ms step).

## 405 Quantifying information dynamic with Transfer Entropy

We first analysed the single-trials activity profiles of each recording site on each recording session for both animals. To remove noise and outliers from our data, we excluded from the analysis the trials for which the SA showed peaks with an amplitude that exceeded the average of the activity by 2 standard deviations in the epoch of interest and for over 80% of the channels. This ensures that artifacts caused by non-physiological oscillations are excluded from the analysis. To examine the local information dynamics in the PMd, we then computed a trial-average time series for each of the SAs recorded by the electrodes of the array for each behavioural condition of each recording session. We then constructed the information transfer network using multivariate Transfer Entropy (*TE*). The choice is due to the fact that TE is indicated (especially in its multivariate formulations) as more accurate compared to other metrics and is known to capture non-linear interaction in the system dynamic without assuming any particular model. Moreover, this measure is of growing interest in neuroscience and there is a thriving literature on it<sup>74-78</sup>. For its computation we used the Matlab *MUTE* toolbox<sup>79</sup>.

Given an ensemble of  $M$  time series, the multivariate information transfer from a *driver* time series  $X$  to a *target* time series  $Y$  (see Figure 8), conditioned to the remaining  $Z_{k=1, \dots, M-2}$  time series, can be quantified taking into account the present values of the target and the past values of both the driver and the  $Z$ <sup>74,79,80</sup> through:

$$TE_{X \rightarrow Y | Z} = H(Y_n | Y_n^-, Z_n^-) - H(Y_n | X_n^-, Y_n^-, Z_n^-), \quad (1)$$

where  $Y_n$  is the vector that represent the present state  $n$  of  $Y$ ,  $X_n^- = [X_{n-1}, X_{n-2}, \dots]$ ,  $Y_n^- = [Y_{n-1}, Y_{n-2}, \dots]$  and  $Z_n^- = [Z_{n-1}, Z_{n-2}, \dots]$  are the vectors that represent the past of  $X$ ,  $Y$  and  $Z$  respectively. The vertical bar stands for conditional probability, e.g.  $H(Y_n | Y_n^-, Z_n^-)$  is the entropy of the present state of  $Y$  conditioned to the knowledge of the past of  $Y$  and to the past of the remaining  $Z$ .  $H$  is the Shannon entropy<sup>81</sup>, which in the case of  $Y$  is given by:

$$H(Y_n) = - \sum_n P(Y_n) \log P(Y_n), \quad (2)$$

where  $P$  indicates the probability density. Hence, using equation 2 expression 1 becomes

$$TE_{X \rightarrow Y | Z} = - \sum_n P(Y_n, Y_n^-, Z_n^-) \log \frac{P(Y_n | X_n^-, Y_n^-, Z_n^-)}{P(Y_n | Y_n^-, Z_n^-)} \quad (3)$$

406 In this formulation *TE* grows if the past of the driver increases the information about the present of target  
 407 more than the past of target itself and more than any other series contained in  $Z$ . Since the past of the  
 408 driver is used to predict the present of the target, TE is not symmetric (i.e.  $TE_{X \rightarrow Y} \neq TE_{Y \rightarrow X}$ ) and  
 409 defines a direction in the information transfer. A crucial issue when estimating TE is the approximation

410 of the vectors representing the past of the time series, a procedure known as *embedding*. The optimal  
411 embedding would be the one that include only the components of  $X_n^-$ ,  $Y_n^-$  and  $Z_n^-$  that are most informative  
412 in describing  $Y_n$ . Montalto et al.<sup>79</sup> described in details different procedures for embedding and to evaluate  
413 the probability distribution functions needed to compute the entropy terms. We opted for a non-uniform  
414 embedding scheme<sup>82</sup> paired with the computation of  $H$  based on kernels estimators<sup>1</sup>. In few words the  
415 embedding method we chose iteratively selects components of the systems past based on a criterion  
416 for maximum relevance and minimum redundancy. In this context, maximum relevance means most  
417 significant in the sense of predictive information. Non-uniform embedding selects from the past of  
418 X, Y and Z only the components that are the most informative for the present of the target variable Y  
419 progressively pruning non informative terms. The maximum number of past values, or maximum lag  $l$ , to  
420 consider for the pruning is fixed at the beginning of the procedure. Cycling through the components of  
421 the past up to  $l$ , the statistical significance is then progressively assessed through the comparison with an  
422 null distribution built from the empirical values via a randomization procedure<sup>79</sup>. The component of the  
423 past of X, Y and Z are thus selected as statistical significant if they are significant above a desired level  $\alpha$ .  
424 In our case the null distribution was obtained by 100 random shuffling of empirical values and we fixed  
425  $\alpha = 0.01$ . Non-uniform embedding represents a convenient and more reliable<sup>74</sup> alternative to the common  
426 used approach known as uniform embedding; this would indeed select the past values  $X_n^-$ ,  $Y_n^-$  and  $Z_n^-$   
427 *a priori* and separately for each time series<sup>79</sup>. The probability density P needed for the computations  
428 of  $H$  was then calculated using kernel functions which weight the distance to the reference point to any  
429 other point in the time series and then average across all points. Such approach computes probabilities  
430 exploiting a local exploring of the state space and, importantly, has been proven to be more robust against  
431 unreliable estimations<sup>74</sup>. Therefore, if at least one component from the past is selected by the non-uniform  
432 embedding procedure, the resulting  $TE_{X \rightarrow Y | Z}$  is positive and statistically significant. When instead none  
433 of the components of the past provide statically significant information about the target the  $TE_{X \rightarrow Y | Z}$  is  
434 exactly 0 and assumed non significant<sup>79</sup>. To avoid any further bias in the selection of the past values, we  
435 initially fixed  $l=50$  ms, but, as expected, only a recent past was selected by the procedure, in line with  
436 similar studies<sup>26,31</sup>. Indeed, for each SA time series, a past no older than 10ms for each  $n$  of equation 2  
437 was ever selected by the optimal embedding procedure.

## 438 Graph theoretical measures

439 In our context the time series were the SAs recorded by the electrodes of the array. We computed  
440  $TE_{X \rightarrow Y | Z}$  (and  $TE_{Y \rightarrow X | Z}$ ) with  $Z_{k=1, \dots, M-2}$ , for each pair of (X, Y) in the epochs defined in Section 1 so  
441 to obtain a  $TE$  matrix<sup>2</sup> for each behavioural condition (Go trials and correct Stop trials) for both monkeys.  
442 Since the purpose of this study was to investigate the topology of information processing within the PMd  
443 cortical network during motor planning and inhibition, we interpreted the asymmetric  $TE$  matrix as the  
444 adjacency matrix of a directed weighted network, in which the nodes are the single modules (channels)  
445 and the weighted edges are the  $TE_{X \rightarrow Y | Z}$  (and  $TE_{Y \rightarrow X | Z}$ ) with  $Z_{k=1, \dots, M-2}$ . To simplify the picture  
446 we considered only the off-diagonal elements of the matrix thus excluding self-loops from the networks.  
447 Figure 8 reports a sketch of the construction of the local TE-based information network. As an initial  
448 skimming of the contribution of each recording site to the exchange of information in the network we  
449 analyzed the empirical TE distributions. We found a mean  $\mu \sim 10^{-2}$  for the TE distributions for all  
450 recording sessions of both behavioural conditions for both animals. Subsequently, we grouped channels

<sup>1</sup>For the complete description of the embedding methods and estimators for computation of  $H$ , which is beyond the scope of this study, see the works of Faes et al.<sup>80,82,83</sup> and references therein.

<sup>2</sup>96x96 for all recording sessions for Monkey P; for some recording sessions of Monkey C damaged channels were removed from the analysis and therefore a 79x79 matrix was obtained.

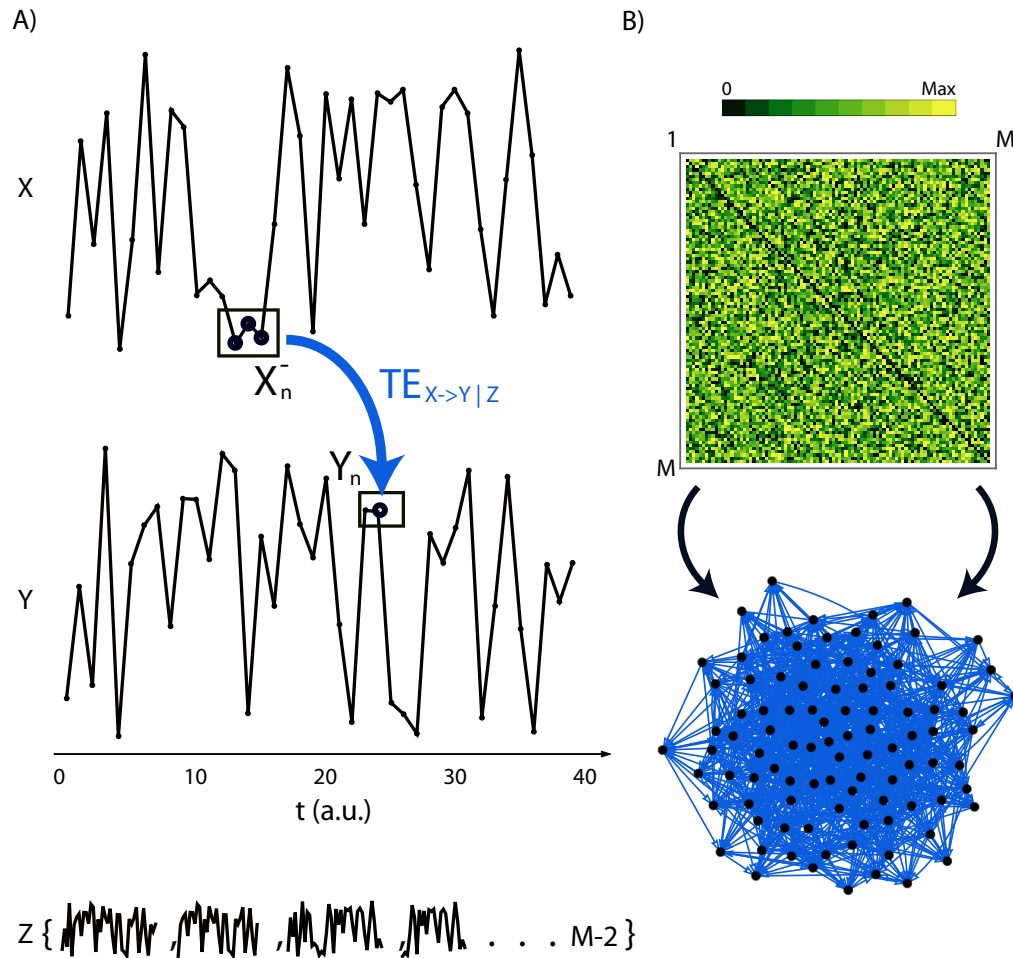


**Figure 8. Sketch of the construction of the local TE-based network given the ensemble of the SA time series. Panel A:** key steps for the computation of the information transfer. For each couple (X,Y) of the ensemble of M time series,  $TE_{X \rightarrow Y | Z}$  quantifies the information transfer from a *driver* X to a *target* Y conditioned to the remaining Z time series, with  $Z_{k=1, \dots, M-2}$  (the same holds for each (Y,X) couple and  $TE_{Y \rightarrow X | Z}$ ). If  $TE_{X \rightarrow Y | Z} \neq 0$  the past of the driver  $X_n^-$  gives more knowledge about the present  $Y_n$  of the target than the past of the target itself and the remaining Z time series, i.e. give statistical significant contribution to the prediction of the present of the target. This defines a hierarchy of information transmission in which the driver is above the target. In this sketch the past of the driver comprises 3 time steps backwards with respect to the reference point and thus  $X_n^- = [X_{n-1}, X_{n-2}, X_{n-3}]$ . **Panel B:** an asymmetric transfer matrix  $M \times M$  can be built computing the terms  $TE_{X \rightarrow Y | Z}$  and  $TE_{Y \rightarrow X | Z}$  for each X and Y of the ensemble. We take the TE matrix to be the adjacency matrix of a directed weighted graph in which the nodes are the channels and the weighted edges are the TE values (for simplicity diagonal elements are taken to be 0 and thus self-loops are excluded).

451 according to the trial type in which they significantly exchanged information with respect to the others.  
 452 To this end we selected from the empirical TE distribution the values  $> \mu + 2\sigma$  for each behavioural  
 453 condition (with  $\sigma$  standard deviation). This selection identified the neuronal classes. As an example  
 454 if node  $i$  drives node  $j$  with a TE value  $> \mu + 2\sigma$  (i.e. there is a strong link directed from  $i$  to  $j$ ) in Go



455 trials but not in correct Stop trials,  $i$  would belong to the Go\_drivers. Interestingly we identified two  
456 peculiar classes: nodes that emitted significant amount of information during both behavioural conditions  
457 (Common\_drivers) and nodes that never emitted information in any behavioral condition (Targets). In our  
458 framework the TE values represented the strength of the connections between network nodes and hence  
459 the above classes are defined based of how much and during which behavioural condition nodes spread  
460 information trough the local PMd network.

461

462 To properly inspect the contribution of each node we needed a set of measures from graph theory. The  
463 first was Vertex Degree (VD). Vertex degree is the number of links to a node  $i$ :

$$VD(i) = \sum_{j=1}^N a_{ij}, \quad (4)$$

464

465 where  $a_{ij}$  is the generic entry of the adjacency matrix and  $N$  is the number of nodes. In directed  
466 networks one can distinguish between in-degree (the number on inward links) and out-degree (the number  
467 of outward links). We computed the probability distribution of both vertex degrees (i.e. the in/out degree  
468 distribution) for each behavioural condition of each recording sessions for both animals. If the variance of  
469 the degree distribution is significantly larger than its mean, tails in the distribution arise and network hubs  
470 are identified (see Figure S1). Hubs are thus nodes that significantly exceeds the average degree of the  
471 network<sup>23</sup>.

472

We further studied the topology of the PMd information network by computing the Betweenness  
Centrality<sup>24,25</sup> (BC) of each node. For each node, BC measure the proportion of shortest paths between  
other couple of nodes  $s$  and  $t$  that pass through it and is defined as<sup>24</sup>:

$$BC(i) = \sum_{s \neq v \neq t} \frac{\sigma_{st}(i)}{\sigma_{st}}, \quad (5)$$

473 , where  $\sigma_{st}(i)$  is the number of shortest paths between  $s$  and  $t$  that pass through  $i$  and  $\sigma_{st}$  the the number  
474 of shortest paths between  $s$  and  $t$ . High BC scores indicate that a node lies on a considerable fraction of  
475 shortest paths connecting pairs of vertices in the graph. Thus, such a node is considered a topological  
476 central node since it plays a crucial role in passing and spreading information trough the network. In  
477 this study we used a normalized version of BC by dividing expression 5 by the normalization factor for  
478 directed graph  $(N-1)(N-2)$  which takes into account the number of ordered pairs of nodes used for  
479 calculation (with  $N$  number of nodes). Then, for each recording sessions, we further scaled the so obtained  
480 BC value by its maximum value across behavioural conditions so that BC spanned the  $[0,1]$  interval.

481 As an overall measure of network comparison we used the centralization index  $C$ . Given a graph measure,  
482  $C$  is the total average difference between the maximum of that measure and the values taken by all other  
483 nodes in the network. I.e., the centralization index of  $VD_{out}$  reads:

$$C_{vd} = \frac{1}{N-1} \sum_{i=1}^N [Max(VD_{out}) - VD_{out}^i], \quad (6)$$

484 where  $VD_{out}^i$  is the vertex out degree of node  $i$ ,  $Max(VD_{out})$  is the maximum  $VD_{out}$  value for the examined  
485 graph and  $N$  is the number of nodes. The same holds for BC. We computed  $C$  for both  $VD_{out}^i$  and BC

486 for each recording session and each behavioural condition for both animals and then averaged over sessions.  
487

In order to compute the total magnitude of information exchanged between the neuronal classes we constructed the following interaction measure  $I$ :

$$I_{ij} = \rho \sum_i^M \sum_j^M \sum_{(m,n)} TE_{C_i^n \rightarrow C_j^m}, \quad (7)$$

488 where  $C$  is the neuronal class,  $M$  is the number of the classes ( $M=4$ ) and  $m$  and  $n$  run over the all possible  
489 combinations of nodes within each class.  $\rho = \frac{\dim(C_i^n \rightarrow C_j^m)}{\dim(C_j)}$  is a normalization factor that accounts for the  
490 heterogeneous number of nodes within each of the classes. Therefore, our  $I_{ij}$  is a normalized node strength  
491 computed on the graph formed by the 4 classes (i.e. in a weighted graph the strength of a node is the sum  
492 of the weights of the links connected to the node). The higher are the number of nodes a class transmits  
493 information to, the higher is  $I$ . Hence, the values and the directions of  $I$  values reflect the position in the  
494 hierarchy of the network communications for that class. All the interactions described by the empirical  
495 TE matrix were thus enclosed in a 4x4 matrix that represents a network of interactions in which now  
496 each node is a neuronal class. We computed  $I$  for each recording session and each behavioural condition  
497 and then we averaged over sessions for both animals. The uncertainty in estimating each element  $I_{ij}$  for  
498 each recording session was given by the standard error. Thus, the sessions-averaged element  $\bar{I}_{ij}$  (Figure 7  
499 and Table 4) is estimated with an error obtained via the error propagation formula for the average of  $n$   
500 measures.

### 501 **A null model**

502 To properly assess the statistical significance of the results obtained via the graph theoretical analysis  
503 we defined a null model. As extensively detailed in a recent work<sup>84</sup>, the choice of a suitable null model  
504 remains a thorny issue in network and complex systems science. One common practice when analysing  
505 real-world networks such the one inspected in the present work, is try to identify properties that deviate  
506 from the null hypothesis being likely that the deviations themselves encode information about the network  
507 functions. In this study we drew our conclusions about the PMd information network in a completely  
508 data-driven fashion directly from neural activity, which thus constituted our only constraint. Therefore,  
509 we tested whether the results were not attributable to the distribution of SA values. To this end we  
510 generated, for each behavioural condition and recording session, a synthetic pool of  $N$  time series with  
511 same length of the empirical ones (with  $N$  number of channels available for the corresponding animal  
512 and recording session) by random sampling from the empirical SA distribution. We then computed the  
513 TE matrix for each synthetic pool. This situation is the most general since assumptions of any kind  
514 are made on the connectivity patterns and the weight distributions of the synthetic networks. We then  
515 compared the empirical graph measures with the ones obtained on the ensemble of 500 randomizations  
516 (see supplementary materials and supplementary figure S4 and S5).

<b><i>VD<sub>Out</sub></i></b>			
<b>Monkey P</b>			
<b>Go trials</b>	Go_drivers	Stop_drivers	Targets
Common_drivers	$Q < 0.005$	$Q < 0.001$	$Q < 0.001$
<b>Stop trials</b>	Go_drivers	Stop_drivers	Targets
Common_drivers	$Q < 0.001$	$Q < 0.01$	$Q < 0.001$
$\Delta_{Stop-Go}$			
Go_drivers	Stop_drivers	Common_drivers	Targets
-98%	+1370%	-18%	-4%
$Q < 0.001$	$Q < 0.001$	$Q > 0.25$	$Q > 0.25$
<b>Monkey C</b>			
<b>Go trials</b>	Go_drivers	Stop_drivers	Targets
Common_drivers	$Q < 0.01$	$Q < 0.001$	$Q < 0.001$
<b>Stop trials</b>	Go_drivers	Stop_drivers	Targets
Common_drivers	$Q < 0.001$	$Q < 0.01$	$Q < 0.001$
$\Delta_{Stop-Go}$			
Go_drivers	Stop_drivers	Common_drivers	Targets
-97%	+9828%	-29%	-950%
$Q < 0.001$	$Q < 0.001$	$Q > 0.25$	$Q > 0.25$

<b><i>BC</i></b>			
<b>Monkey P</b>			
<b>Go trials</b>	Go_drivers	Stop_drivers	Targets
Common_drivers	$Q > 0.05$	$Q < 0.001$	$Q < 0.001$
<b>Stop trials</b>	Go_drivers	Stop_drivers	Targets
Common_drivers	$Q < 0.001$	$Q < 0.001$	$Q < 0.001$
$\Delta_{Stop-Go}$			
Go_drivers	Stop_drivers	Common_drivers	Targets
-89%	+888%	+157%	+183%
$Q < 0.001$	$Q < 0.001$	$Q < 0.001$	$Q < 0.001$
<b>Monkey C</b>			
<b>Go trials</b>	Go_drivers	Stop_drivers	Targets
Common_drivers	$Q < 0.001$	$Q < 0.001$	$Q < 0.001$
<b>Stop trials</b>	Go_drivers	Stop_drivers	Targets
Common_drivers	$Q < 0.001$	$Q > 0.05$	$Q < 0.001$
$\Delta_{Stop-Go}$			
Go_drivers	Stop_drivers	Common_drivers	Targets
-95%	+5180%	+654%	+800%
$Q < 0.001$	$Q < 0.001$	$Q < 0.001$	$Q > 0.25$

**Table 3. Graph metrics details.**

<b><i>I</i> matrix details</b>				
<b>Monkey P</b>				
<b>Go trials</b>	Go_drivers	Stop_drivers	Common_drivers	Targets
Go_drivers	0	1.3 ± 0.1	0	17.5 ± 0.3
Stop_drivers	0	0	0	0
Common_drivers	3.7 ± 0.1	7 ± 0.2	0	42.3 ± 0.4
Targets	0	0	0	0
<b>Stop trials</b>	Go_drivers	Stop_drivers	Common_drivers	Targets
Go_drivers	0	0	0	0
Stop_drivers	2.6 ± 0.2	0	0	17.5 ± 0.6
Common_drivers	2.3 ± 0.2	4.7 ± 0.4	0	25.4 ± 0.6
Targets	0	0	0	0
<b>Monkey C</b>				
<b>Go trials</b>	Go_drivers	Stop_drivers	Common_drivers	Targets
Go_drivers	0	1.1 ± 0.1	0.3 ± 0.003	21 ± 0.5
Stop_drivers	0	0	0	0
Common_drivers	3.4 ± 0.07	10.7 ± 0.2	0	45.3 ± 0.6
Targets	0	0	0	0
<b>Stop trials</b>	Go_drivers	Stop_drivers	Common_drivers	Targets
Go_drivers	0	0	0	0
Stop_drivers	1.9 ± 0.2	0	0	17 ± 0.6
Common_drivers	2.9 ± 0.2	1.4 ± 0.2	0	23.4 ± 0.5
Targets	0	0	0	0

**Table 4.** *I* matrix details.



## 517 **Acknowledgements**

518 Partially supported by grants from Sapienza University and EU FP7 grant 'BrainLeap'

## 519 **Author contributions statement**

520 Must include all authors, identified by initials, for example: F.G, P.P., E.B. and S.F conceived the  
521 experiment, F.G. and P.P. conducted the experiment, G.B. analysed the results. All authors reviewed the  
522 manuscript.

## 523 **Competing interests**

524 (mandatory statement)

525 The corresponding author is responsible for providing a [competing interests statement](#) on behalf of all  
526 authors of the paper. This statement must be included in the submitted article file.

## References

- 527
- 528 1. Hong, G. & Lieber, C. M. Novel electrode technologies for neural recordings. *Nat. Rev. Neurosci.* **20**,  
529 330–345, [10.1038/s41583-019-0140-6](https://doi.org/10.1038/s41583-019-0140-6) (2019).
  - 530 2. Ferraina, S. *et al.* Early Coding of Visuomanual Coordination During Reaching in Parietal Area PEc.  
531 *J. Neurophysiol.* **85**, 462–467, [10.1152/jn.2001.85.1.462](https://doi.org/10.1152/jn.2001.85.1.462) (2001).
  - 532 3. Wurtz, R. H., Sommer, M. A., Paré, M. & Ferraina, S. Signal transformations from cerebral cortex to  
533 superior colliculus for the generation of saccades. *Vis. Res.* **41**, 3399–3412, [10.1016/S0042-6989\(01\)](https://doi.org/10.1016/S0042-6989(01)00066-9)  
534 [00066-9](https://doi.org/10.1016/S0042-6989(01)00066-9) (2001).
  - 535 4. Herreras, O. Local Field Potentials: Myths and Misunderstandings. *Front. Neural Circuits* **10**, 101,  
536 [10.3389/fncir.2016.00101](https://doi.org/10.3389/fncir.2016.00101) (2016).
  - 537 5. Stark, E. & Abeles, M. Predicting movement from multiunit activity. *J. Neurosci.* **27**, 8387–8394,  
538 [10.1523/JNEUROSCI.1321-07.2007](https://doi.org/10.1523/JNEUROSCI.1321-07.2007) (2007).
  - 539 6. Trautmann, E. M. *et al.* Accurate Estimation of Neural Population Dynamics without Spike Sorting.  
540 *Neuron* **103**, 292–308, [10.1016/j.neuron.2019.05.003](https://doi.org/10.1016/j.neuron.2019.05.003) (2019).
  - 541 7. Mattia, M. *et al.* Heterogeneous attractor cell assemblies for motor planning in premotor cortex. *J.*  
542 *Neurosci.* **33**, 11155–11168, [10.1523/JNEUROSCI.4664-12.2013](https://doi.org/10.1523/JNEUROSCI.4664-12.2013) (2013).
  - 543 8. Wise, S. P., Boussaoud, D., Johnson, P. B. & Caminiti, R. Premotor and parietal cortex: Corticocortical  
544 connectivity and combinatorial computations, [10.1146/annurev.neuro.20.1.25](https://doi.org/10.1146/annurev.neuro.20.1.25) (1997).
  - 545 9. Cisek, P. & Kalaska, J. F. Neural mechanisms for interacting with a world full of action choices,  
546 [10.1146/annurev.neuro.051508.135409](https://doi.org/10.1146/annurev.neuro.051508.135409) (2010).
  - 547 10. Shenoy, K. V., Sahani, M. & Churchland, M. M. Cortical Control of Arm Movements: A Dynamical  
548 Systems Perspective. *Annu. Rev. Neurosci.* **36**, 337–359, [10.1146/annurev-neuro-062111-150509](https://doi.org/10.1146/annurev-neuro-062111-150509)  
549 (2013).
  - 550 11. Riehle, A., Grün, S., Diesmann, M. & Aertsen, A. Spike synchronization and rate modulation  
551 differentially involved in motor cortical function. *Science* **278**, 1950–1953, [10.1126/science.278.5345.](https://doi.org/10.1126/science.278.5345.1950)  
552 [1950](https://doi.org/10.1126/science.278.5345.1950) (1997).
  - 553 12. Georgopoulos, A. P., Schwartz, A. B. & Kettner, R. E. Neuronal population coding of movement  
554 direction. *Science* **233**, 1416–1419, [10.1126/science.3749885](https://doi.org/10.1126/science.3749885) (1986).
  - 555 13. Munoz, D. P. & Wurtz, R. H. Fixation cells in monkey superior colliculus I. Characteristics of cell  
556 discharge. *J. Neurophysiol.* **70**, 559–575, [10.1152/jn.1993.70.2.559](https://doi.org/10.1152/jn.1993.70.2.559) (1993).
  - 557 14. Schall, J. D. Visuomotor Functions in the Frontal Lobe. *Annu. Rev. Vis. Sci.* **1**, 469–498, [10.1146/](https://doi.org/10.1146/annurev-vision-082114-035317)  
558 [annurev-vision-082114-035317](https://doi.org/10.1146/annurev-vision-082114-035317) (2015).
  - 559 15. Vaadia, E., Kurata, K. & Wise, S. P. Neuronal activity preceding directional and nondirectional  
560 cues in the premotor cortex of rhesus monkeys. *Somatosens. & Mot. Res.* **6**, 207–230, [10.3109/](https://doi.org/10.3109/08990228809144674)  
561 [08990228809144674](https://doi.org/10.3109/08990228809144674) (1988).
  - 562 16. Fetz, E. E. Are movement parameters recognizably coded in the activity of single neurons? *Behav.*  
563 *Brain Sci.* **15**, 679–690, [10.1017/S0140525X00072599](https://doi.org/10.1017/S0140525X00072599) (1992).
  - 564 17. Vyas, S., Golub, M. D., Sussillo, D. & Shenoy, K. V. Computation through Neural Population  
565 Dynamics, [10.1146/annurev-neuro-092619-094115](https://doi.org/10.1146/annurev-neuro-092619-094115) (2020).

- 566 **18.** Bardella, G., Pani, P., Brunamonti, E., Giarrocco, F. & Ferraina, S. The small scale functional topology  
567 of movement control: Hierarchical organization of local activity anticipates movement generation in  
568 the premotor cortex of primates. *NeuroImage* **207**, [10.1016/j.neuroimage.2019.116354](https://doi.org/10.1016/j.neuroimage.2019.116354) (2020).
- 569 **19.** Giarrocco, F. *et al.* Neuronal dynamics of signal selective motor plan cancellation in the macaque  
570 dorsal premotor cortex. *Cortex* **135**, 326–340, [10.1016/j.cortex.2020.09.032](https://doi.org/10.1016/j.cortex.2020.09.032) (2021).
- 571 **20.** Hubel, D. H. & Wiesel, T. N. Receptive fields, binocular interaction and functional architecture in the  
572 cat's visual cortex. *The J. Physiol.* **160**, 106–154, [10.1113/jphysiol.1962.sp006837](https://doi.org/10.1113/jphysiol.1962.sp006837) (1962).
- 573 **21.** Stuphorn, V. Neural mechanisms of response inhibition, [10.1016/j.cobeha.2014.10.009](https://doi.org/10.1016/j.cobeha.2014.10.009) (2015).
- 574 **22.** Schreiber, T. Measuring information transfer. *Phys. Rev. Lett.* **85**, 461–464, [10.1103/PhysRevLett.85.](https://doi.org/10.1103/PhysRevLett.85.461)  
575 [461](https://doi.org/10.1103/PhysRevLett.85.461) (2000).
- 576 **23.** Albert, R. & Barabási, A.-L. Statistical mechanics of complex networks. *Rev. Mod. Phys.* **74**, 47–97,  
577 [10.1103/RevModPhys.74.47](https://doi.org/10.1103/RevModPhys.74.47) (2002).
- 578 **24.** Freeman, L. C. A Set of Measures of Centrality Based on Betweenness. *Sociometry* **40**, 35,  
579 [10.2307/3033543](https://doi.org/10.2307/3033543) (1977).
- 580 **25.** White, D. R. & Borgatti, S. P. Betweenness centrality measures for directed graphs. Tech. Rep.  
581 (1994).
- 582 **26.** Shimono, M. & Beggs, J. M. Functional clusters, hubs, and communities in the cortical microconnec-  
583 tome. *Cereb. Cortex* **25**, 3743–3757, [10.1093/cercor/bhu252](https://doi.org/10.1093/cercor/bhu252) (2015).
- 584 **27.** Buehlmann, A. & Deco, G. Optimal information transfer in the cortex through synchronization. *PLoS*  
585 *Comput. Biol.* **6**, 1000934, [10.1371/journal.pcbi.1000934](https://doi.org/10.1371/journal.pcbi.1000934) (2010).
- 586 **28.** Orlandi, J. G., Stetter, O., Soriano, J., Geisel, T. & Battaglia, D. Transfer entropy reconstruction and  
587 labeling of neuronal connections from simulated calcium imaging. *PLoS ONE* **9**, 98842, [10.1371/](https://doi.org/10.1371/journal.pone.0098842)  
588 [journal.pone.0098842](https://doi.org/10.1371/journal.pone.0098842) (2014).
- 589 **29.** Ito, S. *et al.* Extending Transfer Entropy Improves Identification of Effective Connectivity in a Spiking  
590 Cortical Network Model. *PLoS ONE* **6**, e27431, [10.1371/journal.pone.0027431](https://doi.org/10.1371/journal.pone.0027431) (2011).
- 591 **30.** Nigam, S. *et al.* Rich-club organization in effective connectivity among cortical neurons. *J. Neurosci.*  
592 **36**, 655–669, [10.1523/JNEUROSCI.2177-15.2016](https://doi.org/10.1523/JNEUROSCI.2177-15.2016) (2016).
- 593 **31.** Timme, N. M. *et al.* High-Degree Neurons Feed Cortical Computations. *PLOS Comput. Biol.* **12**,  
594 e1004858, [10.1371/journal.pcbi.1004858](https://doi.org/10.1371/journal.pcbi.1004858) (2016).
- 595 **32.** Gerhard, F., Pipa, G., Lima, B., Neuenschwander, S. & Gerstner, W. Extraction of Network Topology  
596 From Multi-Electrode Recordings: Is there a Small-World Effect? *Front. Comput. Neurosci.* **5**, 4,  
597 [10.3389/fncom.2011.00004](https://doi.org/10.3389/fncom.2011.00004) (2011).
- 598 **33.** Honey, C. J., Kötter, R., Breakspear, M. & Sporns, O. Network structure of cerebral cortex shapes  
599 functional connectivity on multiple time scales. *Proc. Natl. Acad. Sci. United States Am.* **104**,  
600 10240–10245, [10.1073/pnas.0701519104](https://doi.org/10.1073/pnas.0701519104) (2007).
- 601 **34.** Jahfari, S. *et al.* Effective connectivity reveals important roles for both the hyperdirect (fronto-  
602 subthalamic) and the indirect (fronto-striatal-pallidal) fronto-basal ganglia pathways during response  
603 inhibition. *J. Neurosci.* **31**, 6891–6899, [10.1523/JNEUROSCI.5253-10.2011](https://doi.org/10.1523/JNEUROSCI.5253-10.2011) (2011).
- 604 **35.** Boucher, L., Palmeri, T. J., Logan, G. D. & Schall, J. D. Inhibitory control in mind and brain: An  
605 interactive race model of countermanding saccades. *Psychol. Rev.* **114**, 376–397, [10.1037/0033-295X.](https://doi.org/10.1037/0033-295X.114.2.376)  
606 [114.2.376](https://doi.org/10.1037/0033-295X.114.2.376) (2007).

- 607 **36.** Lo, C. C., Boucher, L., Paré, M., Schall, J. D. & Wang, X. J. Proactive inhibitory control and attractor  
608 dynamics in countermanding action: A spiking neural circuit model. *J. Neurosci.* **29**, 9059–9071,  
609 [10.1523/JNEUROSCI.6164-08.2009](https://doi.org/10.1523/JNEUROSCI.6164-08.2009) (2009).
- 610 **37.** Churchland, M. M. *et al.* Neural population dynamics during reaching. *Nature* **487**, 51–56, [10.1038/  
611 nature11129](https://doi.org/10.1038/nature11129) (2012).
- 612 **38.** Chandrasekaran, C., Peixoto, D., Newsome, W. T. & Shenoy, K. V. Laminar differences in decision-  
613 related neural activity in dorsal premotor cortex. *Nat. Commun.* **8**, 1–16, [10.1038/s41467-017-00715-0](https://doi.org/10.1038/s41467-017-00715-0)  
614 (2017).
- 615 **39.** Kaufman, M. T. *et al.* The largest response component in the motor cortex reflects movement timing  
616 but not movement type. *eNeuro* **3**, 85–101, [10.1523/ENEURO.0085-16.2016](https://doi.org/10.1523/ENEURO.0085-16.2016) (2016).
- 617 **40.** Clawson, W. *et al.* Computing hubs in the hippocampus and cortex. *Sci. Adv.* **5**, eaax4843, [10.1126/  
618 sciadv.aax4843](https://doi.org/10.1126/sciadv.aax4843) (2019).
- 619 **41.** Schroeder, K. E. *et al.* Disruption of corticocortical information transfer during ketamine anesthesia  
620 in the primate brain. *NeuroImage* **134**, 459–465, [10.1016/j.neuroimage.2016.04.039](https://doi.org/10.1016/j.neuroimage.2016.04.039) (2016).
- 621 **42.** Marcos, E. *et al.* Neural variability in premotor cortex is modulated by trial history and predicts  
622 behavioral performance. *Neuron* **78**, 249–255, [10.1016/j.neuron.2013.02.006](https://doi.org/10.1016/j.neuron.2013.02.006) (2013).
- 623 **43.** Verbruggen, F. & Logan, G. D. Response inhibition in the stop-signal paradigm, [10.1016/j.tics.2008.  
624 07.005](https://doi.org/10.1016/j.tics.2008.07.005) (2008).
- 625 **44.** Schall, J. D., Palmeri, T. J. & Logan, G. D. Models of inhibitory control. *Philos. Transactions Royal  
626 Soc. B: Biol. Sci.* **372**, 20160193, [10.1098/rstb.2016.0193](https://doi.org/10.1098/rstb.2016.0193) (2017).
- 627 **45.** Wei, W., Rubin, J. E. & Wang, X. J. Role of the indirect pathway of the basal ganglia in perceptual  
628 decision making. *J. Neurosci.* **35**, 4052–4064, [10.1523/JNEUROSCI.3611-14.2015](https://doi.org/10.1523/JNEUROSCI.3611-14.2015) (2015).
- 629 **46.** Gu, Y., Qi, Y. & Gong, P. Rich-club connectivity, diverse population coupling, and dynamical activity  
630 patterns emerging from local cortical circuits. *PLoS Comput. Biol.* **15**, e1006902, [10.1371/journal.  
631 pcbi.1006902](https://doi.org/10.1371/journal.pcbi.1006902) (2019).
- 632 **47.** Perin, R., Berger, T. K. & Markram, H. A synaptic organizing principle for cortical neuronal groups.  
633 *Proc. Natl. Acad. Sci. United States Am.* **108**, 5419–5424, [10.1073/pnas.1016051108](https://doi.org/10.1073/pnas.1016051108) (2011).
- 634 **48.** Timme, N. *et al.* Multiplex Networks of Cortical and Hippocampal Neurons Revealed at Different  
635 Timescales. *PLoS ONE* **9**, e115764, [10.1371/journal.pone.0115764](https://doi.org/10.1371/journal.pone.0115764) (2014).
- 636 **49.** Schroeter, M. S., Charlesworth, P., Kitzbichler, M. G., Paulsen, O. & Bullmore, E. T. Emergence of  
637 rich-club topology and coordinated dynamics in development of hippocampal functional networks In  
638 vitro. *J. Neurosci.* **35**, 5459–5470, [10.1523/JNEUROSCI.4259-14.2015](https://doi.org/10.1523/JNEUROSCI.4259-14.2015) (2015).
- 639 **50.** Gal, E. *et al.* Rich cell-type-specific network topology in neocortical microcircuitry. *Nat. Neurosci.*  
640 **20**, 1004–1013, [10.1038/nn.4576](https://doi.org/10.1038/nn.4576) (2017).
- 641 **51.** Dann, B., Michaels, J. A., Schaffelhofer, S. & Scherberger, H. Uniting functional network topology  
642 and oscillations in the fronto-parietal single unit network of behaving primates. *eLife* **5**, [10.7554/  
643 eLife.15719](https://doi.org/10.7554/eLife.15719) (2016).
- 644 **52.** Hilgetag, C., O’Neill, M. A. & Young, M. P. Hierarchical organization of macaque and cat cortical  
645 sensory systems explored with a novel network processor. *Philos. Transactions Royal Soc. London.  
646 Ser. B: Biol. Sci.* **355**, 71–89, [10.1098/rstb.2000.0550](https://doi.org/10.1098/rstb.2000.0550) (2000).

- 647 **53.** Hilgetag, C. C. & Kaiser, M. Clustered organization of cortical connectivity, [10.1385/NI:2:3:353](https://doi.org/10.1385/NI:2:3:353)  
648 (2004).
- 649 **54.** Felleman, D. J., Felleman, D. J. & Van Essen, D. C. Distributed hierarchical processing in the primate  
650 cerebral cortex. *CEREB CORTEX* 1–47 (1991).
- 651 **55.** Sporns, O., Tononi, G. & Kötter, R. The Human Connectome: A Structural Description of the Human  
652 Brain. *PLoS Comput. Biol.* **1**, e42, [10.1371/journal.pcbi.0010042](https://doi.org/10.1371/journal.pcbi.0010042) (2005).
- 653 **56.** Kaiser, M. Hierarchy and dynamics of neural networks. *Front. Neuroinformatics* **4**, 112, [10.3389/  
654 fninf.2010.00112](https://doi.org/10.3389/fninf.2010.00112) (2010).
- 655 **57.** Zamora-López. Cortical hubs form a module for multisensory integration on top of the hierarchy of  
656 cortical networks. *Front. Neuroinformatics* **4**, 1, [10.3389/neuro.11.001.2010](https://doi.org/10.3389/neuro.11.001.2010) (2010).
- 657 **58.** Zeki, S. & Shipp, S. The functional logic of cortical connections, [10.1038/335311a0](https://doi.org/10.1038/335311a0) (1988).
- 658 **59.** Tononi, G., Sporns, O. & Edelman, G. M. A measure for brain complexity: Relating functional  
659 segregation and integration in the nervous system. *Proc. Natl. Acad. Sci. United States Am.* **91**,  
660 5033–5037, [10.1073/pnas.91.11.5033](https://doi.org/10.1073/pnas.91.11.5033) (1994).
- 661 **60.** Sporns, O., Honey, C. J. & Kötter, R. Identification and Classification of Hubs in Brain Networks.  
662 *PLoS ONE* **2**, e1049, [10.1371/journal.pone.0001049](https://doi.org/10.1371/journal.pone.0001049) (2007).
- 663 **61.** Watanabe, T. *et al.* Energy landscapes of resting-state brain networks. *Front. Neuroinformatics* **8**, 12,  
664 [10.3389/fninf.2014.00012](https://doi.org/10.3389/fninf.2014.00012) (2014).
- 665 **62.** Kaiser, M., Görner, M. & Hilgetag, C. C. Criticality of spreading dynamics in hierarchical cluster  
666 networks without inhibition. *New J. Phys.* **9**, 110, [10.1088/1367-2630/9/5/110](https://doi.org/10.1088/1367-2630/9/5/110) (2007).
- 667 **63.** Bardella, G., Bifone, A., Gabrielli, A., Gozzi, A. & Squartini, T. Hierarchical organization of  
668 functional connectivity in the mouse brain: A complex network approach. *Sci. Reports* **6**, 1–11,  
669 [10.1038/srep32060](https://doi.org/10.1038/srep32060) (2016).
- 670 **64.** Hilgetag, C. C. & Goulas, A. ‘Hierarchy’ in the organization of brain networks. *Philos. Transactions  
671 Royal Soc. B: Biol. Sci.* **375**, 20190319, [10.1098/rstb.2019.0319](https://doi.org/10.1098/rstb.2019.0319) (2020).
- 672 **65.** Fox, M. D. *et al.* The human brain is intrinsically organized into dynamic, anticorrelated functional  
673 networks. *Proc. Natl. Acad. Sci. United States Am.* **102**, 9673–9678, [10.1073/pnas.0504136102](https://doi.org/10.1073/pnas.0504136102)  
674 (2005).
- 675 **66.** He, B. J. Scale-free properties of the functional magnetic resonance imaging signal during rest and  
676 task. *J. Neurosci.* **31**, 13786–13795, [10.1523/JNEUROSCI.2111-11.2011](https://doi.org/10.1523/JNEUROSCI.2111-11.2011) (2011).
- 677 **67.** Zalesky, A., Fornito, A., Cocchi, L., Gollo, L. L. & Breakspear, M. Time-resolved resting-state brain  
678 networks. *Proc. Natl. Acad. Sci. United States Am.* **111**, 10341–10346, [10.1073/pnas.1400181111](https://doi.org/10.1073/pnas.1400181111)  
679 (2014).
- 680 **68.** Shine, J. M. *et al.* The Dynamics of Functional Brain Networks: Integrated Network States during  
681 Cognitive Task Performance. *Neuron* **92**, 544–554, [10.1016/j.neuron.2016.09.018](https://doi.org/10.1016/j.neuron.2016.09.018) (2016).
- 682 **69.** Vidaurre, D., Smith, S. M. & Woolrich, M. W. Brain network dynamics are hierarchically organized in  
683 time. *Proc. Natl. Acad. Sci. United States Am.* **114**, 12827–12832, [10.1073/pnas.1705120114](https://doi.org/10.1073/pnas.1705120114) (2017).
- 684 **70.** Morcos, A. S. & Harvey, C. D. History-dependent variability in population dynamics during evidence  
685 accumulation in cortex. *Nat. Neurosci.* **19**, 1672–1681, [10.1038/nn.4403](https://doi.org/10.1038/nn.4403) (2016).



- 686 **71.** Logan, G. D. & Cowan, W. B. On the ability to inhibit thought and action: A theory of an act of  
687 control. *Psychol. Rev.* **91**, 295–327, [10.1037//0033-295x.91.3.295](https://doi.org/10.1037//0033-295x.91.3.295) (1984).
- 688 **72.** Band, G. P., van der Molen, M. W. & Logan, G. D. Horse-race model simulations of the stop-signal  
689 procedure. *Acta Psychol.* **112**, 105–142, [10.1016/S0001-6918\(02\)00079-3](https://doi.org/10.1016/S0001-6918(02)00079-3) (2003).
- 690 **73.** Mattia, M. & Del Giudice, P. Population dynamics of interacting spiking neurons. *Phys. Rev. E - Stat.*  
691 *Physics, Plasmas, Fluids, Relat. Interdiscip. Top.* **66**, 19, [10.1103/PhysRevE.66.051917](https://doi.org/10.1103/PhysRevE.66.051917) (2002).
- 692 **74.** Xiong, W., Faes, L. & Ivanov, P. C. Entropy measures, entropy estimators, and their performance  
693 in quantifying complex dynamics: Effects of artifacts, nonstationarity, and long-range correlations.  
694 *Phys. Rev. E* **95**, 1–37, [10.1103/PhysRevE.95.062114](https://doi.org/10.1103/PhysRevE.95.062114) (2017).
- 695 **75.** Wollstadt, P., Martínez-Zarzuola, M., Vicente, R., Díaz-Pernas, F. J. & Wibral, M. Efficient transfer  
696 entropy analysis of non-stationary neural time series. *PLoS ONE* **9**, 102833, [10.1371/journal.pone.](https://doi.org/10.1371/journal.pone.0102833)  
697 [0102833](https://doi.org/10.1371/journal.pone.0102833) (2014).
- 698 **76.** Vicente, R., Wibral, M., Lindner, M. & Pipa, G. Transfer entropy—a model-free measure of effective  
699 connectivity for the neurosciences. *J. Comput. Neurosci.* **30**, 45–67, [10.1007/s10827-010-0262-3](https://doi.org/10.1007/s10827-010-0262-3)  
700 (2011).
- 701 **77.** Wibral, M. *et al.* Transfer entropy in magnetoencephalographic data: Quantifying information flow in  
702 cortical and cerebellar networks. *Prog. Biophys. Mol. Biol.* **105**, 80–97, [10.1016/j.pbiomolbio.2010.](https://doi.org/10.1016/j.pbiomolbio.2010.11.006)  
703 [11.006](https://doi.org/10.1016/j.pbiomolbio.2010.11.006) (2011).
- 704 **78.** Ramos, A. & Macau, E. Minimum Sample Size for Reliable Causal Inference Using Transfer Entropy.  
705 *Entropy* **19**, 150, [10.3390/e19040150](https://doi.org/10.3390/e19040150) (2017).
- 706 **79.** Montalto, A., Faes, L. & Marinazzo, D. MuTE: A MATLAB toolbox to compare established and novel  
707 estimators of the multivariate transfer entropy. *PLoS ONE* **9**, e109462, [10.1371/journal.pone.0109462](https://doi.org/10.1371/journal.pone.0109462)  
708 (2014).
- 709 **80.** Faes, L., Kugiumtzis, D., Nollo, G., Jurysta, F. & Marinazzo, D. Estimating the decomposition of  
710 predictive information in multivariate systems. *PHYSICAL REVIEW E* **91**, 32904, [10.1103/PhysRevE.](https://doi.org/10.1103/PhysRevE.91.032904)  
711 [91.032904](https://doi.org/10.1103/PhysRevE.91.032904) (2015).
- 712 **81.** Shannon, C. E. A Mathematical Theory of Communication. Tech. Rep.
- 713 **82.** Faes, L., Marinazzo, D., Montalto, A. & Nollo, G. Lag-specific transfer entropy as a tool to assess  
714 cardiovascular and cardiorespiratory information transfer. *IEEE Transactions on Biomed. Eng.* **61**,  
715 2556–2568, [10.1109/TBME.2014.2323131](https://doi.org/10.1109/TBME.2014.2323131) (2014).
- 716 **83.** Faes, L., Nollo, G. & Porta, A. Information-based detection of nonlinear Granger causality in  
717 multivariate processes via a nonuniform embedding technique. *Phys. Rev. E - Stat. Nonlinear, Soft*  
718 *Matter Phys.* **83**, 051112, [10.1103/PhysRevE.83.051112](https://doi.org/10.1103/PhysRevE.83.051112) (2011).
- 719 **84.** Cimini, G. *et al.* The statistical physics of real-world networks. *Nat. Rev. Phys.* **1**, 58–71, [10.1038/](https://doi.org/10.1038/s42254-018-0002-6)  
720 [s42254-018-0002-6](https://doi.org/10.1038/s42254-018-0002-6) (2019).